

DIPLOMARBEIT

Modeling, Identification and Control of Ships equipped with Azipod Propulsion Systems

ausgeführt zum Zwecke der Erlangung des akademischen Grades eines
Diplom-Ingenieurs

eingereicht an der Technischen Universität Wien

Fakultät für Maschinenwesen und Betriebswissenschaften

von

Julian Apfelthaler

Matrikelnummer 00826167

unter der Leitung von

Ass. Prof. Dipl.-Ing. Dr.techn. Christoph Hametner

Institut für Mechanik und Mechatronik

Wien, im Jänner 2022

Eidesstattliche Erklärung

Ich habe zur Kenntnis genommen, dass ich zur Drucklegung meiner Arbeit unter der Bezeichnung Diplomarbeit nur mit Bewilligung der Prüfungskommission berechtigt bin. Ich erkläre weiters an Eides statt, dass ich meine Diplomarbeit nach den anerkannten Grundsätzen für wissenschaftliche Abhandlungen selbstständig ausgeführt habe und alle verwendeten Hilfsmittel, insbesondere die zugrunde gelegte Literatur, genannt habe. Weiters erkläre ich, dass ich dieses Diplomarbeitsthema bisher weder im In- noch Ausland (einer Beurteilerin/einem Beurteiler zur Begutachtung) in irgendeiner Form als Prüfungsarbeit vorgelegt habe und dass diese Arbeit mit der vom Begutachter beurteilten Arbeit übereinstimmt.

Wien, im Jänner 2022

Julian Apfelthaler

Abstract

The area of applying control engineering in a hydrodynamic context is increasing in importance by ongoing adoption in the industrial sector, for example in autonomous ship applications and companies have recently started marketing solutions to private consumers.

In this thesis, a workflow for designing and calibrating a model-based dynamic ship control system is proposed and analysed. The workflow consists of a process to parameterise mathematical models to resemble a given ship's nonlinear dynamic behaviour using system identification, followed by using the parameterised models as a basis for a 2-degrees-of-freedom (2-DoF) control system. In the first major part of this thesis the system identification and model parameterisation are analysed. First, a suitable mathematical formulation for nonlinear ship behaviour was obtained from academic literature. A two-pod azimuthing podded propulsion drive configuration was assumed for its versatility but the approach is extensible to other types of propulsion. It was investigated what types of experiments need to be performed in the context of system identification to estimate sets of model parameters that resemble a given ship's dynamics with enough precision to be used in the controller design, as well as how to increase that precision further by supplying the parameter set found using a least-squares approach as an initial point for gradient-descent based optimisation. The results of the identification procedure are then presented and it is shown that a quadratic nonlinear model can be used to approximate higher order nonlinear ship dynamics and that by extending the model with linear terms, a single model can be used to reproduce either linear or nonlinear ship dynamics.

The second major part concerns the process of using the parameterised models to design a control system. A 2-DoF controller was designed and tested in simulations, which consists of an exact-inversion based feedforward part and a full-state feedback controller tuned with a linear-quadratic-regulator approach to accommodate for the system's multi-input-multi-output characteristic by allowing that each DoF can be adjusted separately. Finally, the proposed workflow is validated by using an independently implemented nonlinear and higher-order ship model to generate measurement data for the system identification process, as well as to show that the resulting controller performs well in a simulation that additionally incorporates wind and wave forces as environmental disturbances.

Kurzfassung

Regelungstechnik in einem hydrodynamischen Kontext anzuwenden gewinnt durch die anhaltende Adoption im Industriesektor zunehmend an Bedeutung, beispielsweise durch die Relevanz für Anwendung bei autonomer Schifffahrt. Ferner werden seit kurzem auch Lösungen für Privatkunden angeboten.

In dieser Arbeit wird ein Workflow für die Auslegung eines modellbasierten, dynamischen Regelungssystem für Schiffe präsentiert und analysiert. Der Workflow besteht aus einer Methode, mithilfe von Systemidentifikation mathematische Modelle zu parametrieren, gefolgt von der Nutzung dieser Modelle als Basis für eine Zweifreiheitsgrad-Regelung.

Im ersten Teil der Arbeit wird die Systemidentifikation und Parametrierung analysiert. Erst wurden geeignete mathematische Modelle zur Beschreibung von nichtlinearem Schiffsverhalten aus der akademischen Literatur ausgewählt. Ein zwei-Pod Propellergondel Antriebssystem wurde aus Gründen der Flexibilität angenommen, der Ansatz lässt sich für andere Antriebsarten adaptieren. Es wurde untersucht, welche Arten an Experimenten im Kontext der Systemidentifikation durchgeführt werden müssen, um die Modellparameter mithilfe eines Least-squares Ansatz mit hinreichender Genauigkeit zu schätzen, dass die Modelle für die Reglerauslegung geeignet sind. Außerdem wurde betrachtet, wie sich die Genauigkeit noch steigern lässt, indem man die geschätzten Parameter als Startpunkt für ein gradientenbasiertes Optimierungsverfahren heranzieht. Die Resultate des Identifikationsprozesses werden präsentiert und es wird gezeigt, dass sich mit einem quadratischen nichtlinearen Modell nichtlineare Schiffsdynamiken höherer Ordnung approximieren lassen, sowie dass durch erweiteren des Modells mit linearen Termen ein Modell erzeugt werden kann, welches lineare sowie nichtlineare Schiffsdynamik wiedergeben kann.

Der zweite Teil der Arbeit beschäftigt sich mit dem Prozess, die parametrierten Modelle zur Auslegung eines Regelungssystems zu verwenden. Eine Zweifreiheitsgradregelung wurde ausgelegt, bestehend aus einer inversionsbasierten Vorsteuerung und einer Regelung durch Zustandsvektorrückführung, welche aufgrund der Mehrgrößeneigenschaft des Systems mit einem Linear-Quadratic-Regulator Ansatz ausgelegt wurde, der eine separate Einstellung der einzelnen Freiheitsgrade zulässt. Zuletzt wurde der gesamte Workflow validiert, indem mit vorhandenen nichtlinearen Schiffsmodellen höherer Ordnung Messdaten generiert wurden und der Regler an diesen Modellen in Simulationen getestet wurde, welche außerdem Wind- und Wellenkräfte als Störgrößen enthielten.

Per ardua ad master.

Contents

1	Introduction	7
1.1	Motivation	7
1.2	Problem statement	8
1.3	Thesis structure	8
2	Parameter identification of ship models	9
2.1	Mathematical boat models	9
2.1.1	General considerations	9
2.1.2	Azimuthing podded propulsion system	14
2.1.3	Ship models for identification	15
2.2	Data generation and test models	20
2.3	Experiment design	22
2.4	Parameterisation of the models	27
2.4.1	Cost function	27
2.4.2	Sensitivity and identifiability analysis	28
2.4.3	Initialisation	32
2.4.4	Optimisation procedure	33
2.5	Performance of identified models	37
2.6	System identification summary	45
3	Model based control design	46
3.1	General considerations	46
3.2	Control concepts	46
3.2.1	Pure feedforward	46
3.2.2	Feedback control	47
3.2.3	2-DoF configuration	48
3.3	Modeling environmental forces	49
3.4	Calculation of pod angles and thrusts	51
3.5	Feedforward performance	52
3.6	Feedback control performance	57
3.7	2-DoF configuration performance	61
4	Summary and conclusion	67

1 Introduction

1.1 Motivation

Recent years have seen an increase in the adoption of autonomous ship technologies, from the industrial off-shore oil sector where they originated in the 1960s into other areas such as surveying or undersea cable laying, and even for leisure use on private boats. On the way towards full autonomy, the only slightly more straightforward problem of near-term ship control has to be overcome. One step on the way there are dynamic positioning systems, which are a class of model-based control systems for a ship's propellers and thrusters to have the vessel maintain heading or position, or perform given maneuvers like mooring automatically. The Yamaha Helm Master system is an example of an implementation of a dynamic positioning system, which rigs a suitable small to medium-scale boat to a multi-input-multi-output (MIMO) control system that is operated by a simple joystick and thus makes maneuvers that would otherwise require considerable skill trivial to perform. Figure 1 shows two such maneuvers that the system is able perform by controlling angles and thrusts of three outboard-motors in concert.



Figure 1: Yamaha Helm Master commercial images showing facilitation of a lateral unmooring maneuver (left) and a stationary rotation maneuver (right) by adjusting the outboard motor operating angles and thrusts automatically.

A requirement for this capability is a propulsion system that allows for sufficient degrees of freedom during maneuvering. One such propulsion method

that offers the needed flexibility with regards to force direction are azimuthing podded propulsion drives (see later in figure 4). A ship equipped with two of these drives is theoretically able to generate any desired force direction along the surface to act on the propelled ship, but finding a combination of pod thrusts and angles to generate a specific desired force vector requires a MIMO-control system to perform the required control operations.

1.2 Problem statement

The goal of this thesis is to investigate an approach for designing a model-based MIMO-control system for the application on ships powered by azimuthing propulsion drives. The first problem is finding and parameterising a model in a way that allows for it to be used as a base for controller design. To this end, a mathematical model that accurately reflects dynamic ship behaviour has to be chosen. This choice directly impacts the problem of how to estimate the model's parameters and which experiments need to be performed, as well as how to handle nonlinearities in case nonlinear hydrodynamic behaviour is considered. The next problem is to investigate if any of the parameterised models can be used for the control system in a way that results in acceptable performance while considering inevitable parameterisation and model inaccuracies as well as environmental forces acting onto a simulated ship.

1.3 Thesis structure

The thesis consists of two major parts:

In section 2, a method for finding a suitable mathematical model for describing ship motion and parameterising it using system identification methods on measurement data from different ship simulations is outlined and validated. A short overview of rigid-body kinetics for ships is provided and the assumed propulsion system is described. Then, two models used as the basis for the subsequent controller are discussed in detail. Design of experiment and the measurement data sources are elaborated, followed by a description of the relevant system identification methods and their applicability to the problem. The performance of the identified models is then assessed by comparison to measurement data and validation data.

Section 3 describes the process of using the most suitable of these models as a base to design and implement a control system that can be used for autopilot or dynamic-positioning applications. The components of a 2 degrees of freedom (2-DoF) setup, as well as the mathematical formulations for wind and wave forces for simulation testing are described. The control system is then tested for functionality during environmental conditions in different configurations using simulations of already available ship models and it is shown that the proposed approach leads to promising results.

2 Parameter identification of ship models

2.1 Mathematical boat models

2.1.1 General considerations

Since boatsmanship is one of humanity's oldest and historically most significant modes of transportation, a sizable amount of literature is available. This section attempts to concisely present the relevant modern definitions and approaches used in this thesis and to put the conducted work into context.

Rigid body kinetics generally allow for a bodies' motion to be described in 6 degrees of freedom, but depending on the application and its required complexity/precision, the scope of the model can be reduced. Using Newton-Euler equations and resorting to the SNAME notation [1] which is the de-facto standard in academic literature on marine hydrodynamics, the equations of motion for constant mass and center of gravity located at (x_g, y_g, z_g) can be derived and are shown in eq. (1).

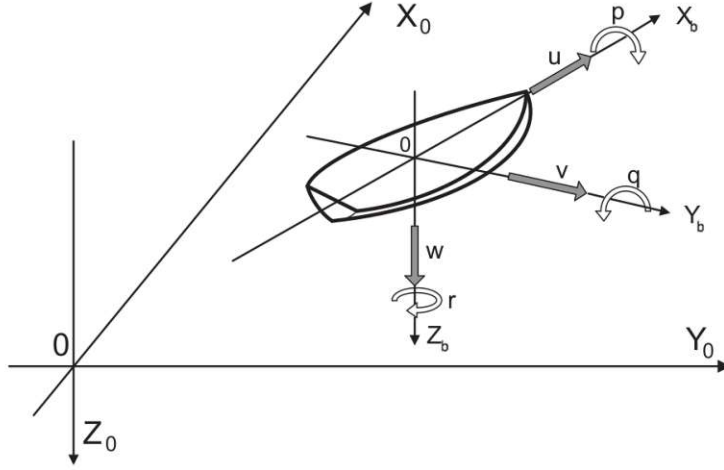


Figure 2: Coordinate systems and SNAME notation to designate a ship's body-fixed axes and velocities.

$$\begin{aligned}
 m[\dot{u} - vr + wq - x_g(p^2 + r) + y_g(pq - \dot{r}) + z_g(pr + \dot{q})] &= \tau_x \\
 m[\dot{v} - wp + ur - y_g(r^2 + p^2) + z_g(qr - \dot{p}) + x_g(qp + \dot{r})] &= \tau_y \\
 m[\dot{w} - uq + vp - z_g(p^2 + q^2) + x_g(rp - \dot{q}) + y_g(rq + \dot{p})] &= \tau_z \\
 I_x \dot{p} + (I_z - I_y)qr - (\dot{r} + pq)I_{xz} + (r^2 - q^2)I_{yz} + (pr - \dot{q})I_{xy} \\
 + m[y_g(\dot{w} - uq + vp) - z_g(\dot{v} - wp + ur)] &= \tau_k \\
 I_y \dot{q} + (I_x - I_z)rp - (\dot{p} + qr)I_{xy} + (p^2 - r^2)I_{zx} + (qp - \dot{r})I_{yz} \\
 + m[z_g(\dot{u} - vr + wq) - x_g(\dot{w} - uq + vp)] &= \tau_m \\
 I_z \dot{r} + (I_y - I_x)pq - (\dot{q} + rp)I_{yz} + (q^2 - p^2)I_{xy} + (rq - \dot{p})I_{zx} \\
 + m[x_g(\dot{v} - wp + ur) - y_g(\dot{u} - vr + wq)] &= \tau_n
 \end{aligned} \tag{1}$$

u, v, w	Velocities in surge, sway and heave.
p, q, r	Angular velocities in roll, pitch and yaw.
$\dot{u}, \dot{v}, \dot{w}$	Accelerations in surge, sway and heave.
$\dot{p}, \dot{q}, \dot{r}$	Angular accelerations in roll, pitch and yaw.
x_g, y_g, z_g	Coordinates of ship's center of gravity.
m	Ship's mass.
I_x, I_y, I_z	Ship's moments of inertia.
I_{xy}, I_{yz}, I_{zx}	Ship's products of inertia.
τ_x, τ_y, τ_z	External forces.
τ_k, τ_m, τ_n	External moments.

Figure 2 shows the orientation of the principal axes relative to a ship's hull in a body-fixed coordinate system. From eq. (1) and according to [2], the following classification of models by starting with the full 6-DoF case and then reducing the number of modeled DoFs depending on the requirements of the application is possible:

- 6-DoF models (surge, sway, heave, roll, pitch and yaw) for full simulation and prediction of ship motion.
- 3-DoF models can themselves be subdivided into:
 - Horizontal plane models (surge, sway and yaw) used in dynamic positioning systems and trajectory-tracking control systems.
 - Longitudinal models (surge, heave and pitch) for forward speed, diving processes for submersibles and pitch control.
 - Lateral models (sway, roll and yaw) for turning and heading control.
- 4-DoF models (surge, sway, roll and yaw) are usually 3-DoF plane models with added roll motions. The roll motion is of importance for investigations into passenger comfort or ship stability, especially under load conditions.

- 1-DoF models for the implementation of simple speed controllers, heading autopilots or roll damping systems.

The focus of this work is to create a control system for performing maneuvers such as mooring or rotations on the spot. Thus, for the purpose of designing this dynamic positioning system, heave, roll and pitch are disregarded and 3-DoF horizontal plane models in surge, sway and yaw were used, specifically and mostly in the formulation used by [3]:

$$\begin{aligned}\dot{u} &= \frac{(m + m_y)vr + \tau_x}{m + m_x} \\ \dot{v} &= \frac{-(m + m_x)ur + \tau_y}{m + m_y} \\ \dot{r} &= \frac{\tau_n}{I_z + i_{zz}}\end{aligned}\tag{2}$$

$$\boldsymbol{\tau} = \boldsymbol{\tau}_{prop} + \boldsymbol{\tau}_{hyd} + \boldsymbol{\tau}_{wind} + \boldsymbol{\tau}_{waves} + \dots$$

m_x, m_y, i_{zz}	Added mass terms.
τ_x, τ_y, τ_n	Generalised forces and moment along principal axes.
τ_{prop}	Propulsion forces.
τ_{hyd}	Hydrodynamic resistance forces.

This formulation assumes, that the ship's body-fixed coordinate system is fixed to its center of gravity, with the x-axis pointing towards the bow. The forces in $\boldsymbol{\tau}$ can incorporate any relevant phenomenon that influences a ship's behaviour, the most important ones for this project being the propulsion forces τ_{prop} , the ship hull's hydrodynamic resistance τ_{hyd} , wind forces τ_{wind} and wave forces τ_{wave} . SI units can be used throughout the whole model.

The hydrodynamic forces τ_{hyd} demand special consideration. There exists a wide variety of approaches to model individual phenomena such as vortex drag, wave drift damping etc., by deriving mathematical formulations of the respective effects from first principles. Another more pragmatic approach, proposed by [4], is to formulate the hydrodynamic resistance terms along the principal axes as a truncated Taylor-series expansion and fitting measurement data into the resulting model to determine the coefficients numerically. Depending on the model application and according to [2], different orders of the Taylor series

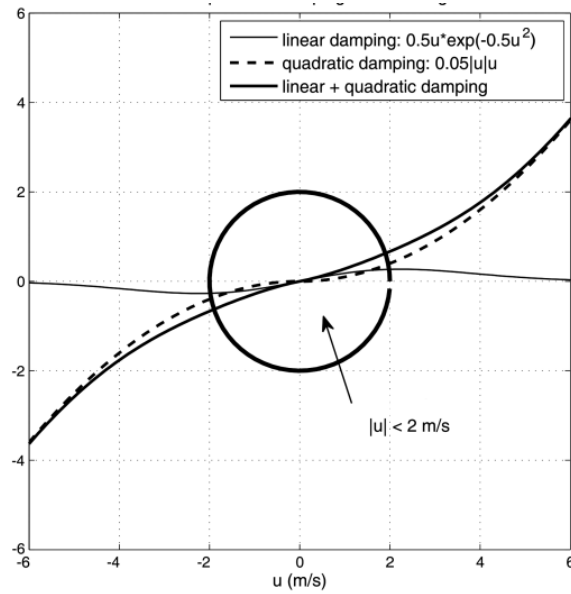


Figure 3: Speed regimes for linear and quadratic hydrodynamic damping.

can be considered, for instance for maneuvering speeds $< 2\text{m/s}$, the linear and quadratic formulations produce similar results at the cost of the linearised model's ability to display oscillatory behaviours. Figure 3 from the same source shows how the linear formulation can be used to approximate the nonlinear one, provided a vessel operates at low enough speed. Even though the assumed use case in this work would fall into that regime, the linearised models turned out to be insufficient for predicting the dynamics of higher-order ship models as shown in section 2.5 and are therefore not used for controller design.

Lastly, the effects of the displaced fluid when a volume moving through it changes its relative velocity are factored into the model. This concept, which is known as "added mass" and "added inertia" is incorporated by adding the extra terms m_x , m_y and i_{zz} .

2.1.2 Azimuthing podded propulsion system

As method of propulsion, a dual azimuth-thruster configuration is assumed, which consists of two thrusters as seen in figure 4 at the stern of the ship that can each rotate 360°. Compared to less flexible methods of propulsion like traditional outboard motors which have an angle of operation of $< 180^\circ$, the operating angle allows for a whole range of options for control design.



Figure 4: Azimuthing podded propulsion drive.

For the ship simulations in this thesis, this means that the propulsion forces are idealised as two freely pivotable force vectors acting on the stern of the ship in the xy -plane. Furthermore, it is assumed that the dynamic behaviour of the propulsion system itself can be neglected and that it is possible to generate any desired force magnitude and direction timeseries within reasonable limits, while in reality the propulsion forces are influenced by factors such as relative speed to the fluid and exhibit dynamic behaviour of their own with regards to engine characteristics and reaction time to inputs. Approaches for modeling the generated forces of podded propulsion in greater detail as well as interactions between multiple pods being operated on the same vessel can be found for example in [5].

The chosen approach of using the generalised force vector τ not only simplifies

the implementation of the models in simulation, but also has the advantage of being freely extensible to different types of propulsion as long as force vectors can be modeled. These can then be easily transformed into a τ_{prop} formulation via equilibrium of forces. The inverse problem, encountered when determining required control inputs for a desired τ_{prop} , generally leads to an overdetermined system of equations, for which a possible solution based on a constrained least-squares approach is described later in section 3.4.

2.1.3 Ship models for identification

Two models were analysed in this work to be used as a basis for the dynamic positioning system. The two ships which the models are originally based on are the "Lanxin USV" unmanned surface vehicle described by Sun et al. [6] and the training ship "Dorchester Lady" described by W. Gierusz [3] and were chosen for analysis because their full mathematical structure and parameterisation was readily available in literature. As shown in figure 5, the two ships differ significantly in size which means differences in motion dynamic behaviour are expected.



Figure 5: The Lanxin USV research ship and the Dorchester Lady training ship.

The Lanxin USV model assumes linear hydrodynamic damping and no coupling-effects between any of the principal axes and will from here on be referred to as model A.

The equations of model A from the paper are given as

$$\dot{u} = \frac{m_{22}}{m_{11}}vr - \frac{d_{11}}{m_{11}}u + \frac{1}{m_{11}}\tau_x \quad (3)$$

$$\dot{v} = -\frac{m_{11}}{m_{22}}ur - \frac{d_{22}}{m_{22}}v + \frac{1}{m_{22}}\tau_y \quad (4)$$

$$\dot{r} = \frac{m_{11} - m_{22}}{m_{33}}uv - \frac{d_{33}}{m_{33}}r + \frac{1}{m_{33}}\tau_n \quad (5)$$

m_{11}, m_{22}, m_{33} Generalised mass terms.

d_{11}, d_{22}, d_{33} Linear hydrodynamic damping coefficients.

The assumptions of linear hydrodynamic damping and no coupling effects result in the model containing only 6 parameters that define its dynamic behaviour, which in the original paper were estimated through recursive least-squares estimation. The ignored hydrodynamic coupling effects specifically lead to behaviour in which motion along one axis is only induced if there are forces acting along that axis which in reality does not hold true for classic v-shaped ship hulls.

The Dorchester Lady model contains only nonlinear hydrodynamic damping terms and motions along any of the axes have an effect on all the other ones, this second model will be referred to as model B.

$$\dot{u} = \frac{(m_{y,tot})vr + \tau_x}{m_{x,tot}} + \frac{1}{m_{x,tot}} \left[\frac{1}{2} \rho_w L T [X_{uu}u|u| + X_{vv}v^2 + L^2 X_{rr}r^2] + X_{vr}vr \right] \quad (6)$$

$$\dot{v} = \frac{-(m_{x,tot})ur + \tau_y}{m_{y,tot}} + \frac{1}{m_{y,tot}} \frac{1}{2} \rho_w L^2 [Y_{vu}v|u| + Y_{vv}v|v| + LY_{ru}r|u| + L^2 Y_{rr}r|r| + LY_{vr}v|r| + LY_{rv}r|v|] \quad (7)$$

$$\dot{r} = \frac{\tau_n}{I_{z,tot}} + \frac{1}{I_{z,tot}} \frac{1}{2} \rho_w L^3 [N_{vu}v|u| + N_{vv}v|v| + LN_{ru}r|u| + L^2 N_{rr}r|r| + LN_{vr}v|r| + LN_{rv}r|v|] \quad (8)$$

- $m_{x,tot}, m_{y,tot}$ Ship mass and added mass.
 $I_{z,tot}$ Moment of inertia and added inertia.
 L Length of ship.
 T Draft.
 ρ_w Density of water.
 X_{ij}, Y_{ij}, N_{ij} Nonlinear hydrodynamic resistance coefficients.

This model contains 19 parameters that were originally found using semi-empirical formulas and the equations are coupled across the 3 axes. Furthermore, in the above formulation some parameters are tied to the same combination of variables, for example $\frac{m_{y,tot}}{m_{x,tot}}$ and X_{vr} in eq. (6) are both tied to the product vr . To prevent ambiguity during the subsequent system identification process by preventing those parameters from being estimated independent of each other and for easier implementation of the model in MATLAB, the parameters were rearranged and combined with coefficients into a new set of parameters θ_1 to θ_{19} as shown in eqs. (9) to (11).

$$\dot{u} = \underbrace{\frac{m_{y,tot} + X_{vr}}{m_{x,tot}}}_{\theta_1} vr + \underbrace{\frac{1}{m_{x,tot}} \frac{1}{2} \rho_w L T X_{uu}}_{\theta_2} u|u| + \underbrace{\frac{1}{m_{x,tot}} \frac{1}{2} \rho_w L T X_{vv}}_{\theta_3} v^2 + \underbrace{\frac{1}{m_{x,tot}} \frac{1}{2} \rho_w T L^3 X_{rr}}_{\theta_4} r^2 + \underbrace{\frac{1}{m_{x,tot}}}_{\theta_5} \tau_x \quad (9)$$

$$\dot{v} = \underbrace{\frac{-(m_{x,tot})}{m_{y,tot}}}_{-\frac{\theta_{12}}{\theta_5}} ur + \underbrace{\frac{1}{m_{y,tot}} \frac{1}{2} \rho_w L^2 Y_{vu}}_{\theta_6} v|u| + \underbrace{\frac{1}{m_{y,tot}} \frac{1}{2} \rho_w L^2 Y_{vv}}_{\theta_7} v|v| + \underbrace{\frac{1}{m_{y,tot}} \frac{1}{2} \rho_w L^3 Y_{ru}}_{\theta_8} r|u| + \underbrace{\frac{1}{m_{y,tot}} \frac{1}{2} \rho_w L^4 Y_{rr}}_{\theta_9} r|r| + \underbrace{\frac{1}{m_{y,tot}} \frac{1}{2} \rho_w L^3 Y_{vr}}_{\theta_{10}} v|r| + \underbrace{\frac{1}{m_{y,tot}} \frac{1}{2} \rho_w L^3 Y_{rv}}_{\theta_{11}} r|v| + \underbrace{\frac{1}{m_{y,tot}}}_{\theta_{12}} \tau_y \quad (10)$$

$$\dot{r} = \underbrace{\frac{1}{I_{z,tot}} \frac{1}{2} \rho_w L^3 N_{vu}}_{\theta_{13}} v|u| + \underbrace{\frac{1}{I_{z,tot}} \frac{1}{2} \rho_w L^3 N_{vv}}_{\theta_{14}} v|v| + \underbrace{\frac{1}{I_{z,tot}} \frac{1}{2} \rho_w L^4 N_{ru}}_{\theta_{15}} r|u| + \underbrace{\frac{1}{I_{z,tot}} \frac{1}{2} \rho_w L^5 N_{rr}}_{\theta_{16}} r|r| + \underbrace{\frac{1}{I_{z,tot}} \frac{1}{2} \rho_w L^4 N_{vr}}_{\theta_{17}} v|r| + \underbrace{\frac{1}{I_{z,tot}} \frac{1}{2} \rho_w L^4 N_{rv}}_{\theta_{18}} r|v| + \underbrace{\frac{1}{I_{z,tot}}}_{\theta_{19}} \tau_n \quad (11)$$

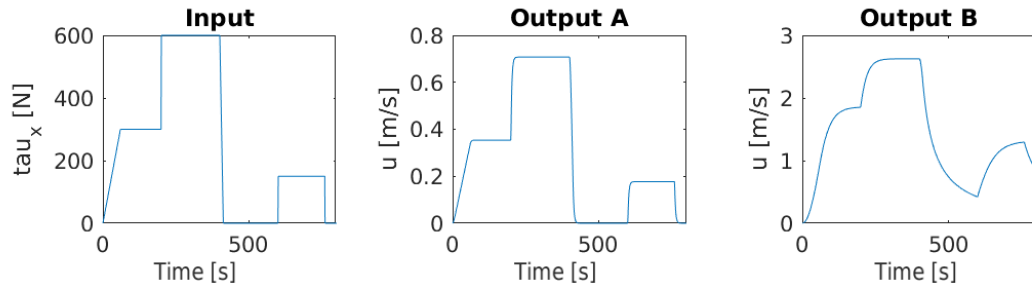


Figure 6: Propulsion step input in surge direction and velocity u outputs of Lanxin USV/model A and Dorchester Lady/Model B.

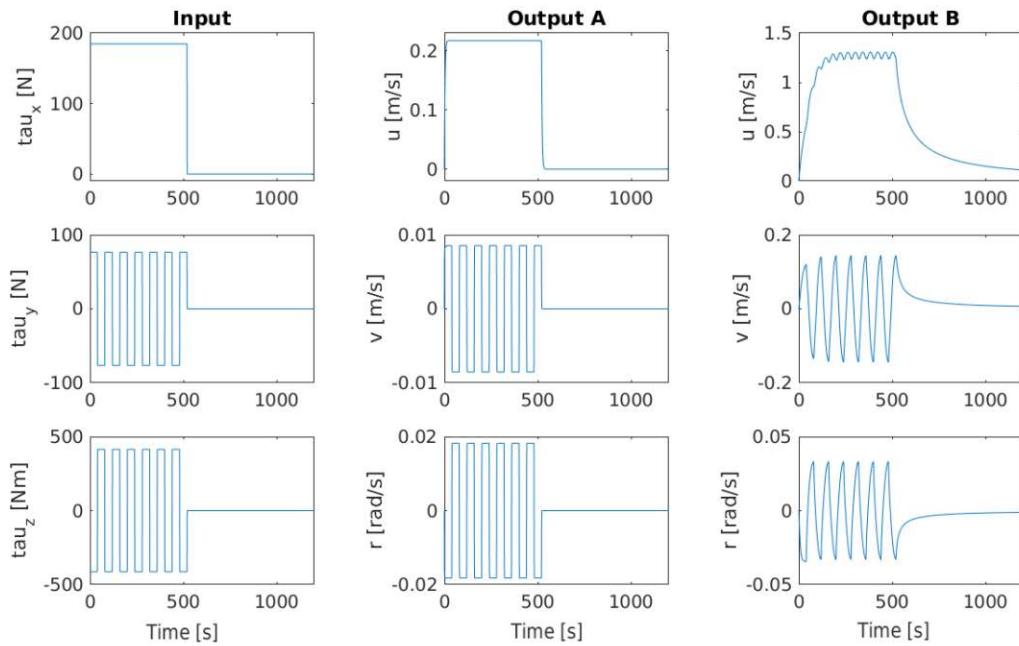


Figure 7: Zigzag-course input and velocity u, v, r outputs of models A and B.

A comparison to show the difference in dynamics between model A and model B is shown in figures 6 and 7. Model A shows a linear relationship between

model input and the resulting steady-state velocities while model B exhibits nonlinear behaviour. Another difference are relatively symmetric acceleration and deceleration properties of the output for the linear case of model A, while for the nonlinear model B there is a strong asymmetry and the velocity slowly decays towards zero in the absence of a propulsion force.

Finally, to analyse the performance of a model that incorporates assumptions about both linear and nonlinear hydrodynamic damping effects, the respective linear damping terms from model A and nonlinear ones from model B were combined into model C, as shown in eqs. (12)-(14).

$$\dot{u} = \theta_1 u + \theta_2 u|u| + \theta_3 v^2 + \theta_4 r^2 + \theta_5 vr + \theta_6 \tau_x \quad (12)$$

$$\dot{v} = -\frac{\theta_{15}}{\theta_6} ur + \theta_7 v + \theta_8 r + \theta_9 v|u| + \theta_{10} v|v| + \theta_{11} r|u| + \theta_{12} r|r| + \theta_{13} v|r| + \theta_{14} r|v| + \theta_{15} \tau_y \quad (13)$$

$$\dot{r} = \theta_{16} v + \theta_{17} r + \theta_{18} v|u| + \theta_{19} v|v| + \theta_{20} r|u| + \theta_{21} r|r| + \theta_{22} v|r| + \theta_{23} r|v| + \theta_{24} \tau_n \quad (14)$$

In this model, the hydrodynamic forces between sway and yaw direction are coupled, which results in the linear terms for v and r appearing in both equations (13) and (14). This combination of linear and nonlinear terms is a valid approach according to [2]. Since the model in this form is not parameterised for any ship in particular, no examples are provided here, but identification results and performance are later shown in chapter 2.5.

2.2 Data generation and test models

In order to validate the approach on independently generated data, experiments were performed using Thor Fossen's Marine System Simulator (MSS)[7], which is a Matlab and Simulink library containing relevant scripts and tools, as well as several fully implemented marine craft models. The two models that were used for testing and verification of the dynamic positioning system are the supply ship and the naval vessel model, which are themselves based on real-life measurements. The supply ship model assumes low maneuvering speeds and thus only contains linear hydrodynamic damping. The naval vessel on the other hand is a 4-DoF model, which includes a degree of freedom to

represent rolling motions of the ship, and it also contains quadratic and cubic hydrodynamic damping terms. The roll-motion was simulated but it was assumed to be unknown to the models used for identification as well as the control system, which effectively turned it into an additional slight uncertainty the control system encounters when applied to the naval vessel model.

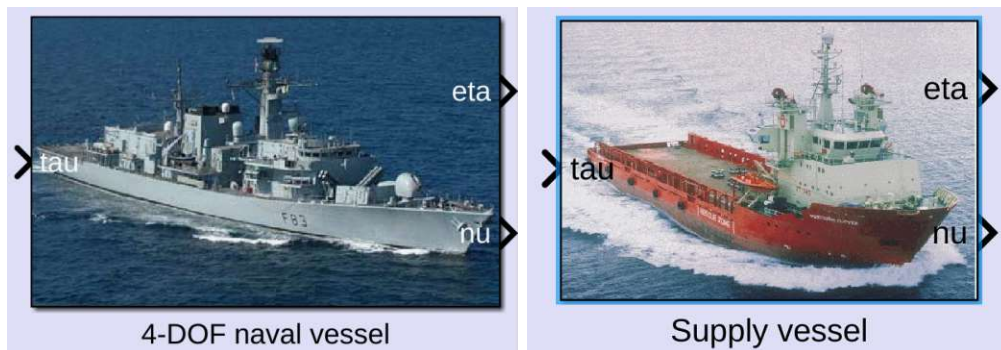


Figure 8: The MSS Simulink blocks containing images of the naval vessel and supply ship.

As seen in figure 8, the two ships are two different classes of vessels and are therefore again expected to behave differently regarding their dynamic characteristics. A comparison of the two models that shows their dynamic behaviour for different maneuvers is found in figures 9 and 10, note the differently scaled velocities in comparison to figures 6 and 7 since the naval vessel and supply ship models are parameterised for much larger craft than the models described in the previous section.

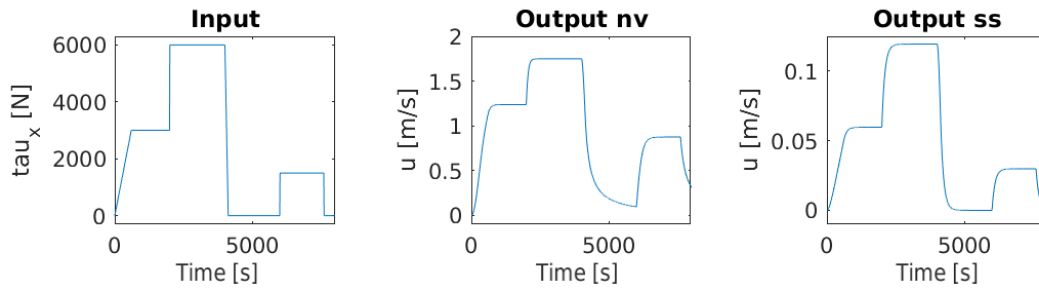


Figure 9: Propulsion step input in surge direction and velocity u outputs of the naval vessel (nv) and supply ship (ss) models.

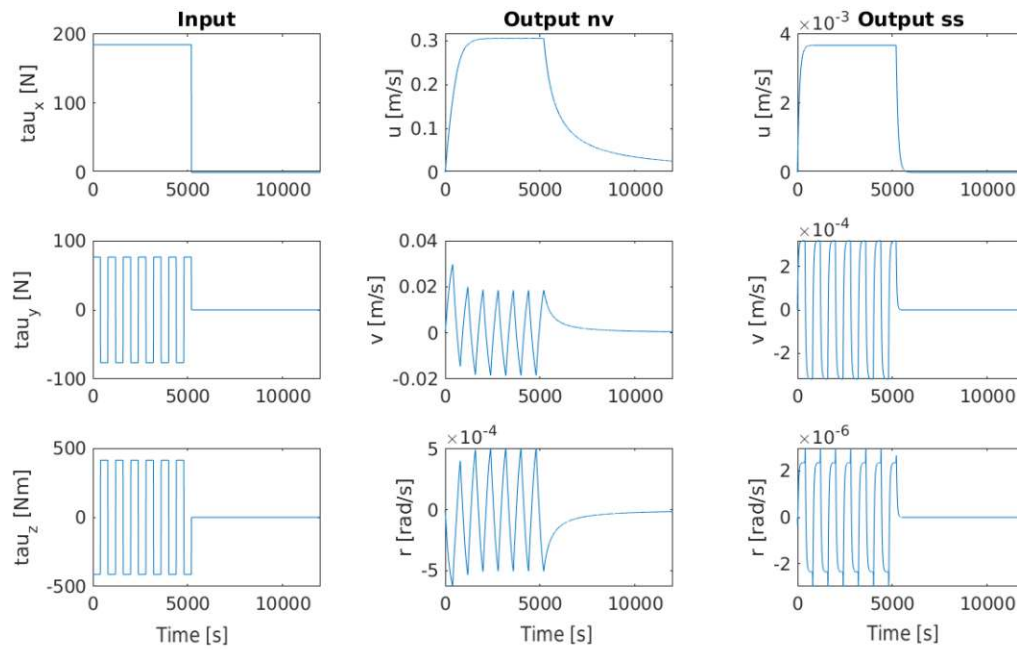


Figure 10: Zigzag-course input and velocity u, v, r outputs of the naval vessel (nv column) and supply ship (ss column) models. Note the inverted turning direction on the supply ship as a result of the hydrodynamic resistance in sway direction.

2.3 Experiment design

In this section, the maneuvers used in the system identification process and the reasoning behind them are discussed. In order to identify the parameters

of models A, B and C described in section 2.1.3 in a way that the identified model can be used as a base for feedback- and feedforward control, the measurements have to be performed in such a way, that the relevant coefficients are being sufficiently excited. Fundamentally, this requirement depends on the models mathematical structure, with more complex models containing more and nonlinear parameters requiring more and more complex experiments.

The maneuvers are designed in a way that incorporates a reasonable balance between dynamic and steady states of the system. The reason for this can be shown for example in equation (3) when one assumes a steady-state ($\dot{u}, \dot{v}, \dot{r} = 0$) of the system, in which case m_{11} couldn't possibly be determined. Standard maneuvers for ship testing used in literature are for example straight-ahead acceleration and coast-downs, zig-zag course or turning maneuvers [8]. The zig-zag course maneuver in particular, which was already shown in figures 7 and 10, is a staple system identification maneuver for ship models that are designed for forward cruising applications and oftentimes a few variations of it are enough data to parameterise a model to accurately perform most forward and turning maneuvers, but this approach failed to produce models that can perform lateral mooring motions or stationary turns. Therefore, a handful of additional measurements were performed in an attempt to sufficiently excite the relevant coefficients, especially concerning motion along sway and yaw direction.

The following section showcases the test-set of 10 experiments chosen to validate the method. Figures 11 to 20 show the original output data from the simulation and the same data with added white noise on the left. As a sensor setup containing a GPS receiver was found to be used for a similar application in literature [9], a signal-to-noise ratio (SNR) of 40 was used to simulate measurement noise levels of GPS receivers similar to those that appear in other publications [10]. On the right are plots of the maneuvers and the path of the ship's coordinate origin in the x-y plane. All experiments shown here were performed with model B as originally parameterised in [3].

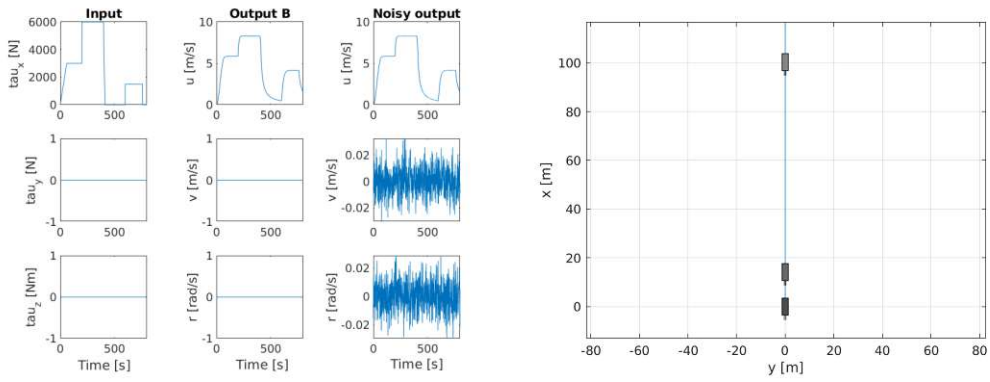


Figure 11: Straight-ahead accelerations and coast-downs.

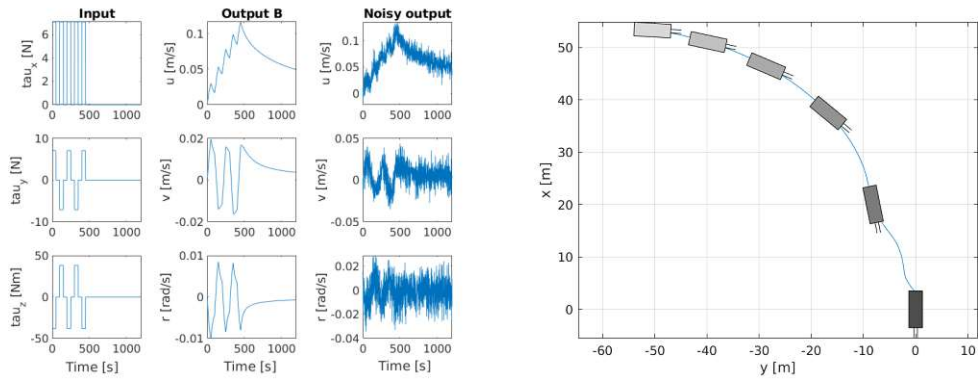


Figure 12: Zigzag-course with coasts in between thrusts and a coast-down at the end.

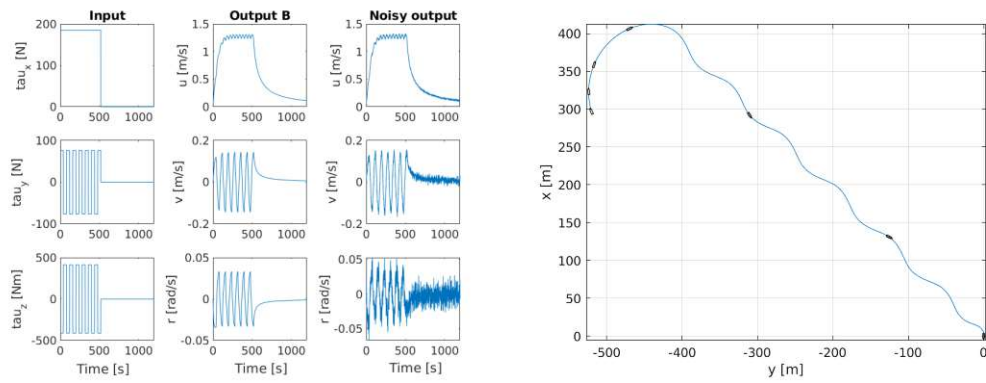


Figure 13: Zigzag-course and coast-down.

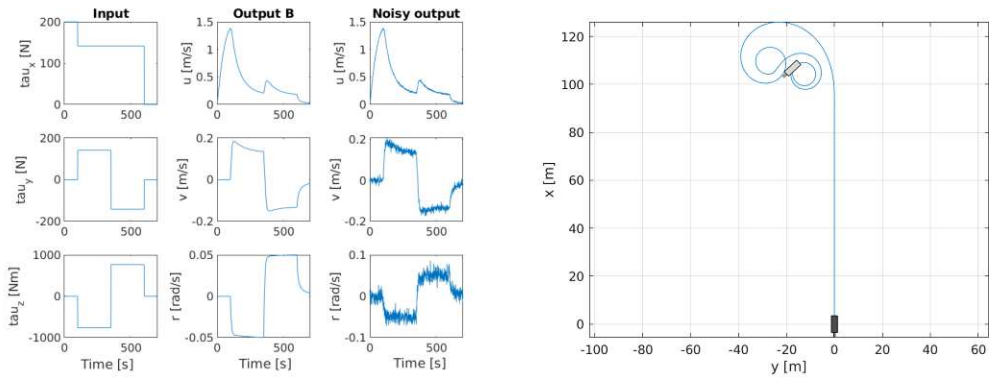


Figure 14: Turning maneuver in both directions.

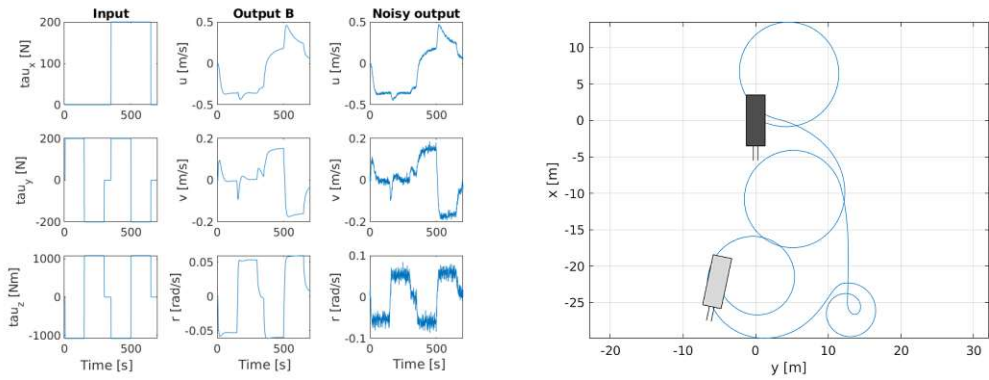


Figure 15: Maneuver that excites u, v and r velocities to a similar magnitude.

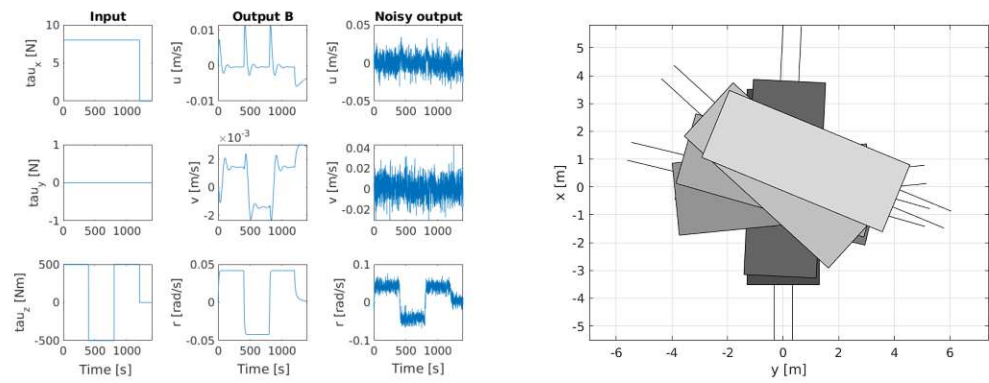


Figure 16: Stationary rotations in both directions.

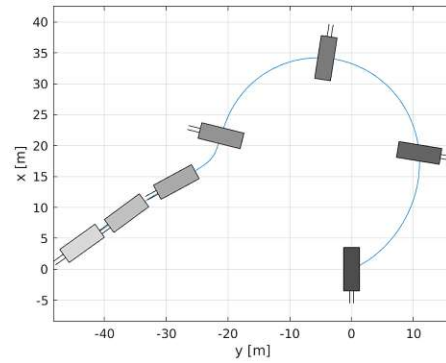
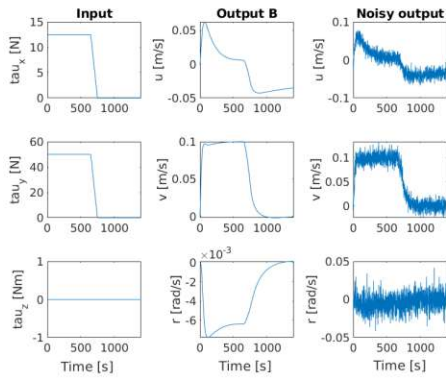


Figure 17: Approximate lateral drift with subsequent coast-down.

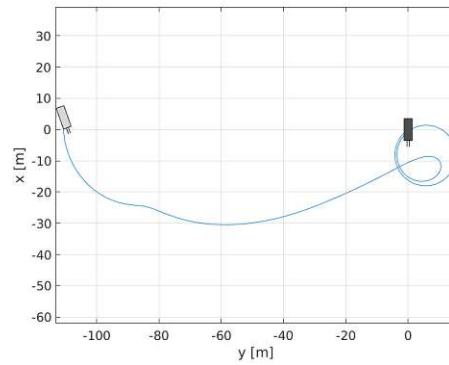
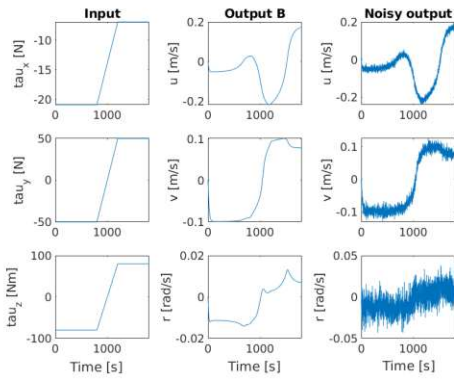


Figure 18: Rotations during lateral- and forward thrust.

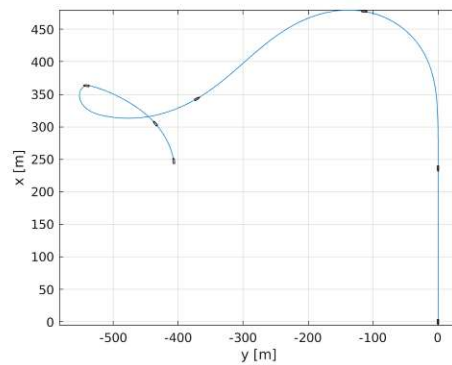
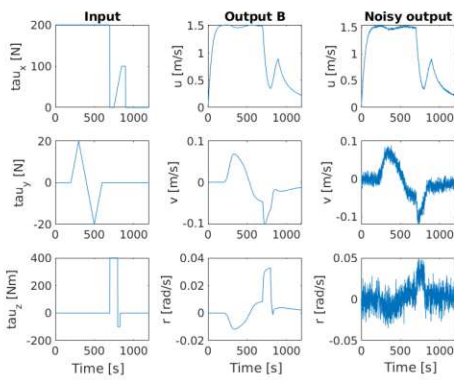


Figure 19: General cruising with some turns during forward thrust.

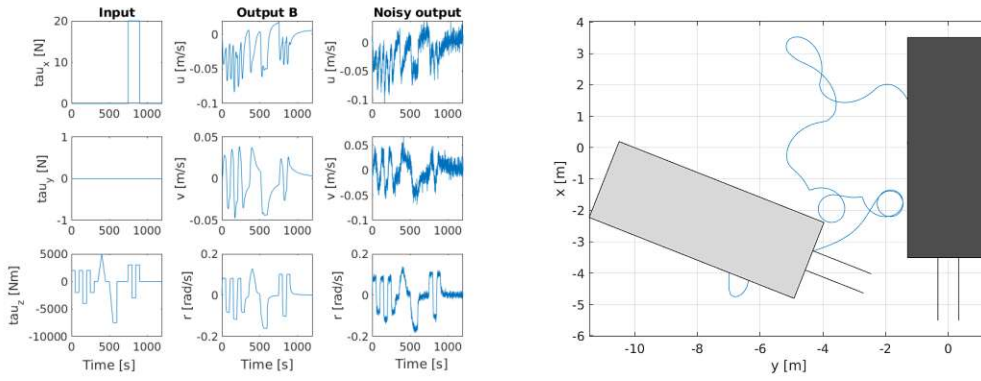


Figure 20: Experiment to emphasise steady-state as well as dynamic behaviour around the rotation axis.

2.4 Parameterisation of the models

2.4.1 Cost function

When designing a model-based controller, one first needs a parameterised ID model to approximate the dynamic behaviour of the ship for which it is to be used. This was done using the established approach of minimising the quadratic error between measurement data and ID model output. To quantify the performance of any set of a models parameters, a simulation was performed and the results were evaluated into a scalar value according to the quadratic cost function [11] with added weights

$$J = \sum_{k=1}^n q_u(u_k - \hat{u}_k)^2 + q_v(v_k - \hat{v}_k)^2 + q_r(r_k - \hat{r}_k)^2 \quad (15)$$

where u_k, v_k, r_k are the n sampled velocity measurements of the conducted experiments, $\hat{u}_k, \hat{v}_k, \hat{r}_k$ are the simulated velocities sampled with the same frequency and q_u, q_v, q_r are the corresponding weight coefficients for the respective axes. When using the cost function to perform optimisation, the weights can be used to tune the influence of any of the three axes on the resulting value, for example to scale the deviations across all experiments in different axes to approximately the same magnitude since the forward, lateral and rotational velocities differ numerically by nature of the system. To capture the relevant time-constants of naval vessel behaviour without either slowing down the op-

timisation process with too great amounts of data or leading to numerical problems during simulation, a sampling time of $T_s = 1\text{Hz}$ proved to be sufficient and was used throughout the whole work.

Further problems that arise during the system identification process are the nonlinearities in the models that were used, estimating an initial set of parameters to approximate the measured dynamics and the question of whether it is possible to optimise the identification model's performance from there. These will be discussed in detail in the following sections.

2.4.2 Sensitivity and identifiability analysis

Parameter sensitivity

Using the cost function described above, sensitivity analysis can be performed to verify the suitability of the chosen mathematical model structures to the problem of approximating a given ship's measured dynamics as well as the feasibility of using gradient descent approaches for further optimisation. The parameter sensitivity is defined as the change of the output, i.e. the measured velocities, with respect to variations of parameters for a given experiment (or set of experiments) and this change can be quantified by using the cost function (15). Conversely, this means a parameter that results in a bigger change of the cost function value relative to others when varied has a bigger influence on the resulting performance, while parameters that only affect the cost function minimally or not at all are of smaller significance or even superfluous, again within the context of the considered experiment(s). This principle is also the basis for gradient descent based optimisation methods, which attempt to minimise the cost function value by varying the parameters systematically.

For our exemplary one-factor-at-a-time analysis, individual parameters of model B were multiplied by evenly spaced factors from 10^{-1} to 10 and the cost function was evaluated for the whole set of 10 experiments to verify the existence of a global cost function minimum at the original parameter values. The plots for parameters 1 and 7 are shown in figure 21 as examples to represent the results: All parameters except 6 and 7 show a similar behaviour to parameter 1 with a clearly visible minimum at their original value, while for parameters 6 and 7 the evaluation of experiment 8 exhibits a possible local minimum where a gradient descent method could potentially get stuck in. This analysis verifies

the existence of a global minimum for all parameters in the context of evaluating the cost function for the set of 10 experiments shown in section 2.3.

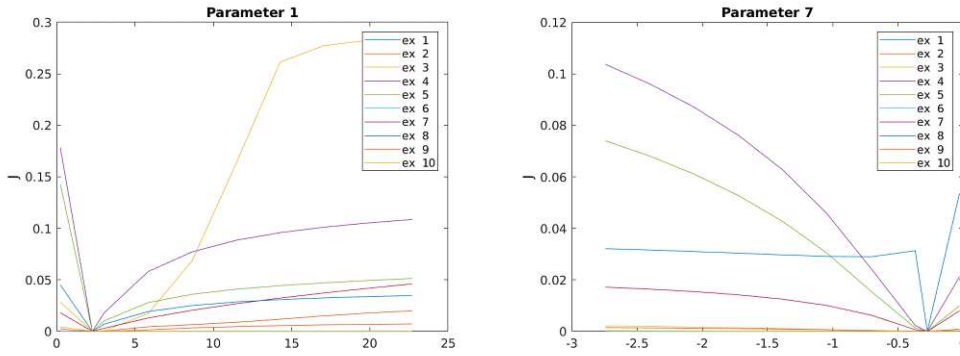


Figure 21: Cost function values for all 10 experiments during one-factor-at-a-time variations of the original value (the cost function minimum) for parameters 1 and 7 of model B.

Monte-carlo analysis

Next, to analyse whether the initially varied parameters actually converge back towards their original values (i.e. their global minimum) during gradient-descent optimisation or drift away from them, a monte-carlo simulation was performed in which each parameter in the set of initial values was randomly varied by $\pm 50\%$ of its original value, followed by gradient-descent optimisation. The gradient-descent method used in this thesis, MATLAB's `fmincon`, is described in more detail in later in section 2.4.4. The results of 100 optimisation runs for model B with the parameter structure of eqs. (9)-(11) are shown in figure 22. There it is apparent, that while most parameters converge to their original value over the course of optimisation, parameters 3, 9, 14, 17 and 18 don't show that behaviour but instead diverge somewhat from their global minima.

The reason for this phenomenon is either parameter drift, the solver arriving at a local minimum or that the influence of those parameters on the cost

function is too small for the optimisation algorithm to detect. This last behaviour can be caused by several factors, one being that the relevant terms for the respective parameters are not being sufficiently excited, either by their influence being indiscernible through the measurement noise or by the set of experiments lacking that excitation in the first place. Additionally, while performing system identification on ships, the problem of multi-collinearity and subsequent parameter drift may arise as described for instance in [12].

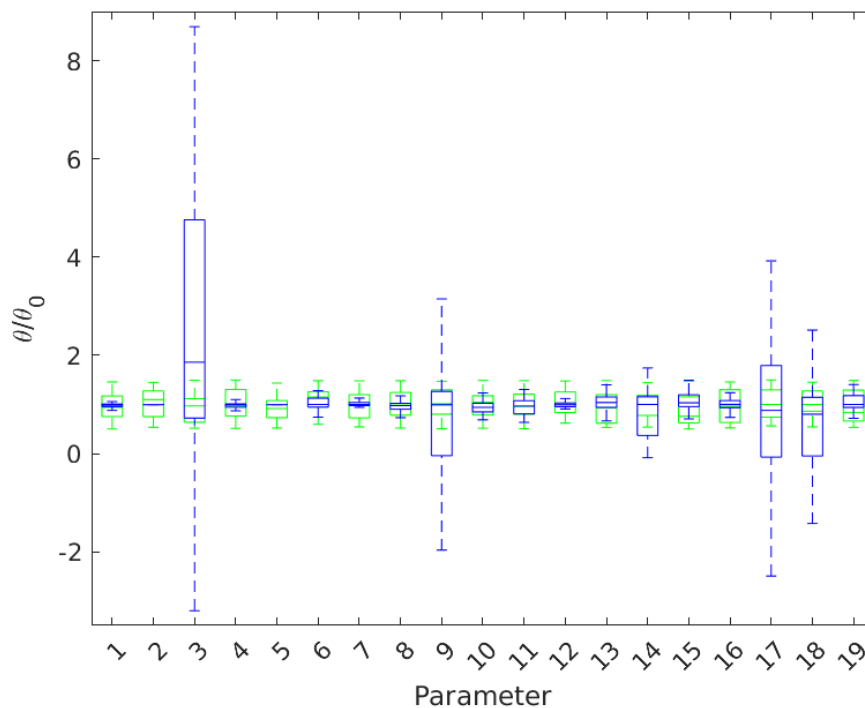


Figure 22: Distribution of ID results for each model parameter from a monte-carlo analysis of 100 optimisation runs. The green boxes show the spread of initial values ($\pm 50\%$ of original value) and the blue ones the spread of the results after optimisation.

While the 5 parameters that didn't converge towards their global minima ap-

parently were not able to be accurately identified given the set of experiments used, in practice this means that for the maneuvers contained in the experiments these parameters show only negligible influence on the results, i.e. the sensitivity of the output with regard to changes of these parameters is low. Therefore, as long as the experiments approximately cover all relevant types of motion, the models should be accurate enough for use in the subsequent control system.

A comparison between one of the best and one of the worst fits of the monte-carlo analysis' results is seen in figure 23 and more in-depth analysis on the implemented control system's performance will be shown in chapter 3. These results show, that given an initial set of parameters close to a global optimum, gradient-descent optimisation generally produces a set of resulting parameters that approximate the dynamics of the test models used.

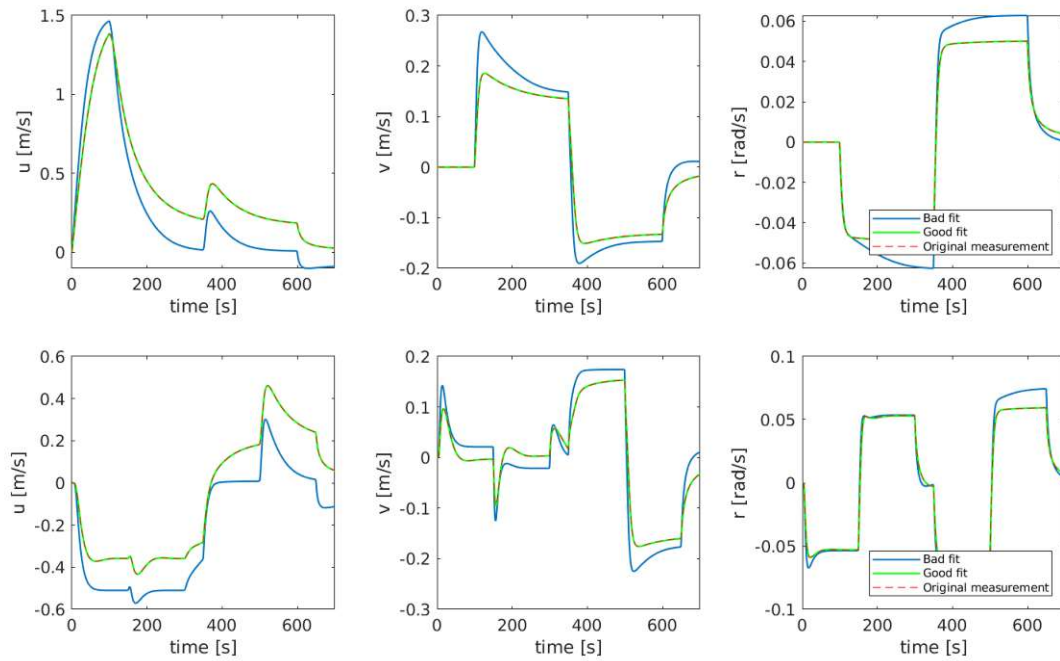


Figure 23: Comparison between one of the lowest and one of the highest fit results of the monte-carlo analysis for experiments 4 and 5, model B.

2.4.3 Initialisation

One method to parameterise the chosen ID-models as described in section 2.4.1 is using gradient-descent optimisation to find a cost function minimum by varying the parameters. For any gradient-descent method, a vector (or range) of initial values has to be provided as a starting point to begin the descent from and this choice of an initial point has a significant effect on the quality of the results. The monte-carlo analysis shown in section 2.4.2 was performed for a system with known parameters and initialised by varying the parameters randomly by $\pm 50\%$ of their original values. For an unknown ship with unknown parameter values, an approach to estimate an initial point is required. Tests were conducted on the use of semi-empirical methods, where the hydrodynamic coefficients are approximated by using formulas dependent on a ship's key metrics like length and draft, as for example discussed in [13]. While those tests sometimes produced results that were adequate for simulations of straight-ahead or zig-zag maneuvers, they generally failed to provide a set of parameters that reflected the measurement's dynamics across all principal axes as well as initial points from which a gradient-descent optimisation could improve on the results.

A proven method to fit parameters of a model onto measured data is least squares estimation. When given enough measurement data, the least squares estimate for all the parameters resulted in a model that resembles the behaviour of the measurements to a high degree without the need to solve differential equations and, for model A and B where the original parameters are known from the literature, the estimates corresponded to the global minima. The first of two possible drawbacks of this approach is that there is no way of determining a minimum set of experiments that are required since the quality of the estimation is not only dependent on the considerations in section 2.3, i.e. that variations of the coefficients need to have a quantifiable effect on the system dynamics for a given experiment, but also the amount of measurement noise and in further consequence on the precision of the acceleration data which is assumed to be found by taking the first derivative of the velocity measurements. The second drawback is, that in case that the supplied measurement data turn out to be insufficient for usable estimates, these estimates would probably not only not be close to an optimal point but so far off that gradient descent methods might get stuck in a local minimum that may be impractical for our application. While these inherent properties of least

squares estimation might lead to problems when using the proposed method, in practice the set of 10 experiments described above proved to be sufficient to produce reasonably useful results, provided the excitations were discernible from the added measurement noise.

2.4.4 Optimisation procedure

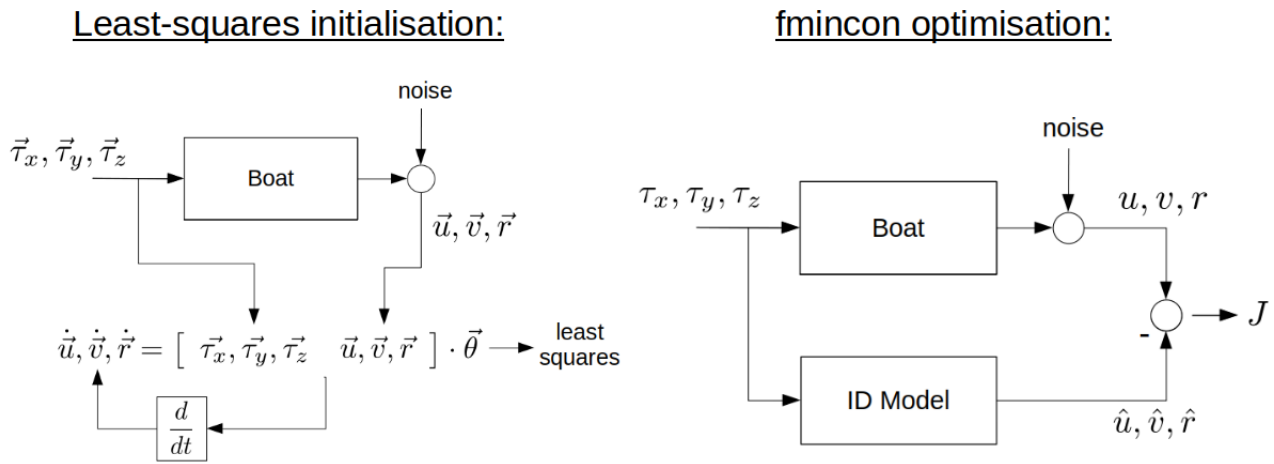


Figure 24: Comparison of the least-squares initialisation and the gradient-based optimisation approach for finding parameters for the identification model.

While the least-squares approach discussed above usually provides a set of parameters that make the chosen ID-model approximate the dynamics of the measurements, there is often room for improvement with regards to precision of the simulation or unwanted oscillatory behaviour. This set of parameters can then be supplied as an initial point for gradient-descent based optimisation methods to further improve upon the result. This is possible because while the least-squares method only minimises the equation error when trying to find a solution for the problem of finding parameters that fit the data, a gradient-descent approach minimises the simulation error as quantified by the cost function. A comparison of the two approaches is shown in figure 24.

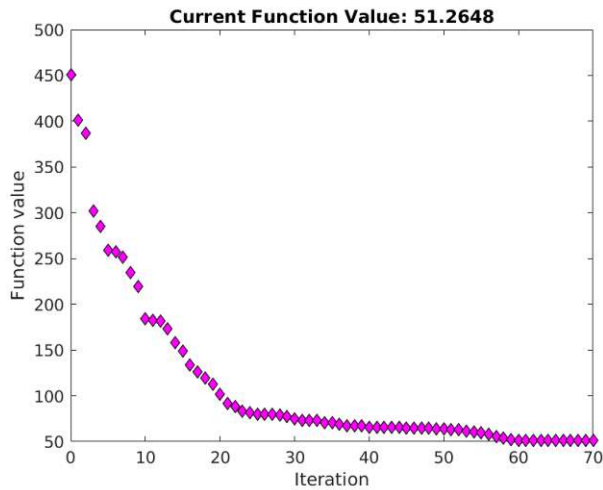


Figure 25: Exemplary progression of cost function values using `fmincon` over the course of a single optimisation run.

The optimisation method used in this thesis is MATLAB’s `fmincon`, a sophisticated algorithm designed for nonlinear problems with continuous objective functions. One issue that arose during this process are instabilities of the system caused by the algorithm guessing parameter values that lead to singularities during simulation, which can be avoided by catching the errors and punishing the cost function by returning big values in case they occur. Also, the optimisation problem was normalised, i.e. the solver started with a vector of ones corresponding to the least-squares initial values that was recalculated into parameter-values at every simulation, to make it numerically easier for the algorithm. `Fmincon` along with these tweaks proved to be a reliable way of finding parameters that can be used as the basis for our model-based control system later. An exemplary progression of cost function values during an optimisation run is shown in figure 25. Exemplary results of the optimisation process for some training experiments are shown in figure 26 and a validation on non-training data in figure 27. These show, that while the least-squares method used on only the measurement data gives a set of parameters that results in a rough approximation by magnitude that still lacks precision, a subsequent application of `fmincon` using these parameters as initial point leads to a very good approximation of the target dynamic behaviour.

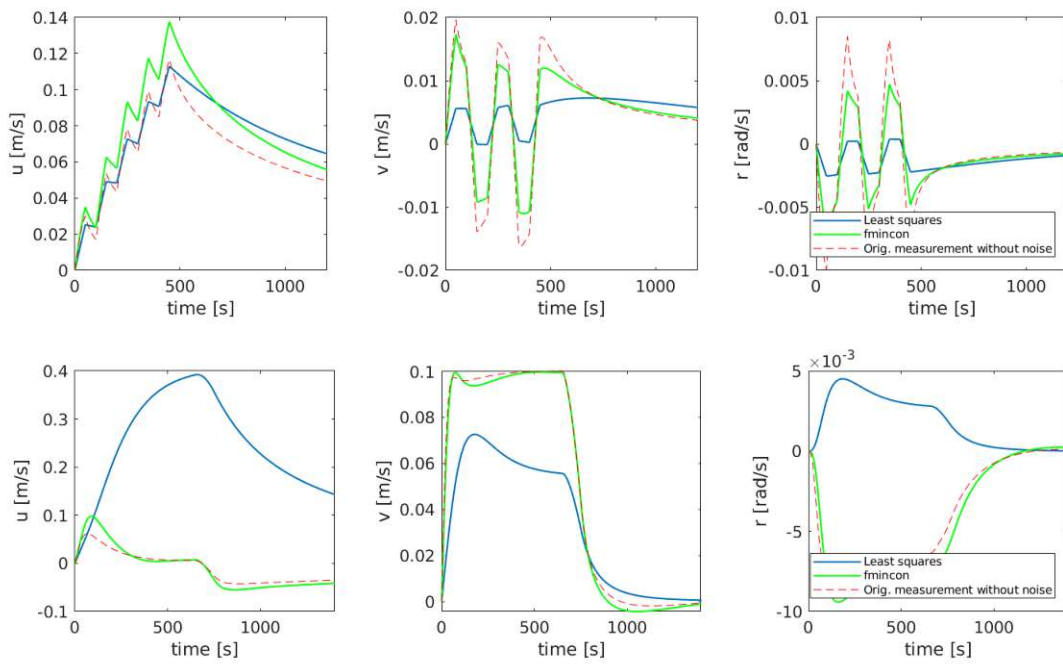


Figure 26: Comparison between least-squares initialisation and fmincon final result for the "zig-zag course with coasts" experiment (top) and the "lateral drift and coast" experiment for model B.

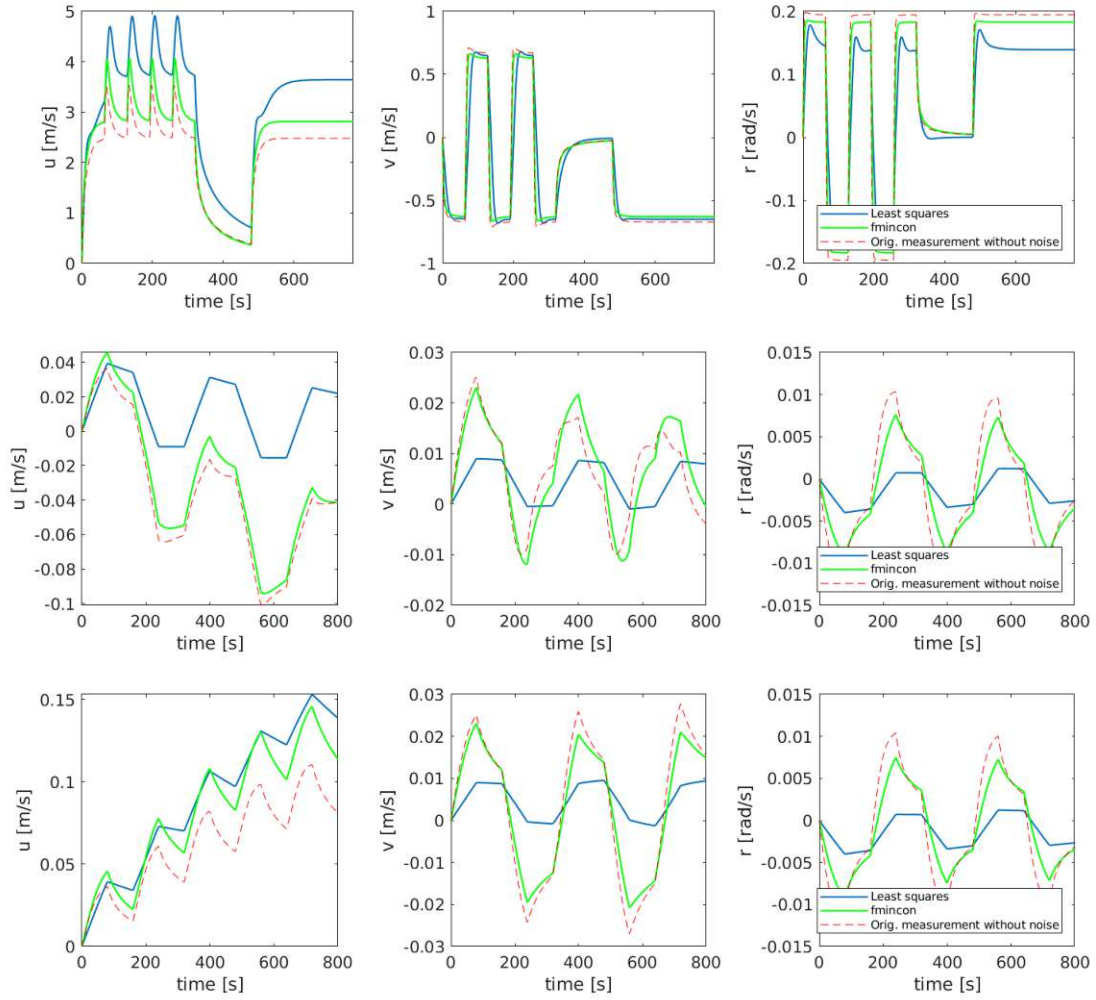


Figure 27: Validation of the identified model on different zig-zag course experiments that were not part of the training set.

2.5 Performance of identified models

This section summarises the results of the system identification process for several relevant combinations of ID-model and measurement data. All identifications were carried out using noisy measurement data in the form of the 10 experiments described above with a signal-to-noise ratio of 40, except for the supply ship experiments for which it had to be doubled since otherwise its slow movements weren't discernible from the noise. The acceleration time-series were then obtained by taking the derivative of moving-average smoothed velocity measurements.

Additionally, model validation similar to the one shown in figure 27 was performed with data not used for the initialisation/optimisation process for all model-data combinations that produced feasible results (A-A, B-nv, C-nv and C-ss). All models performed with approximately the same accuracy as the corresponding exemplary results shown in their respective sections.

Model A

To validate the general functionality of the used methods and the identifiability of the parameters of model A, tests were carried out using measurement data generated with model A itself. Results from this process are shown in figure 28.

Since model A contains only linear and especially uncoupled hydrodynamic resistance terms and is therefore mathematically unable to reflect nonlinear hydrodynamics, identification of data generated using models containing higher-order hydrodynamic resistance gives nonsatisfactory results as shown in figure 29.

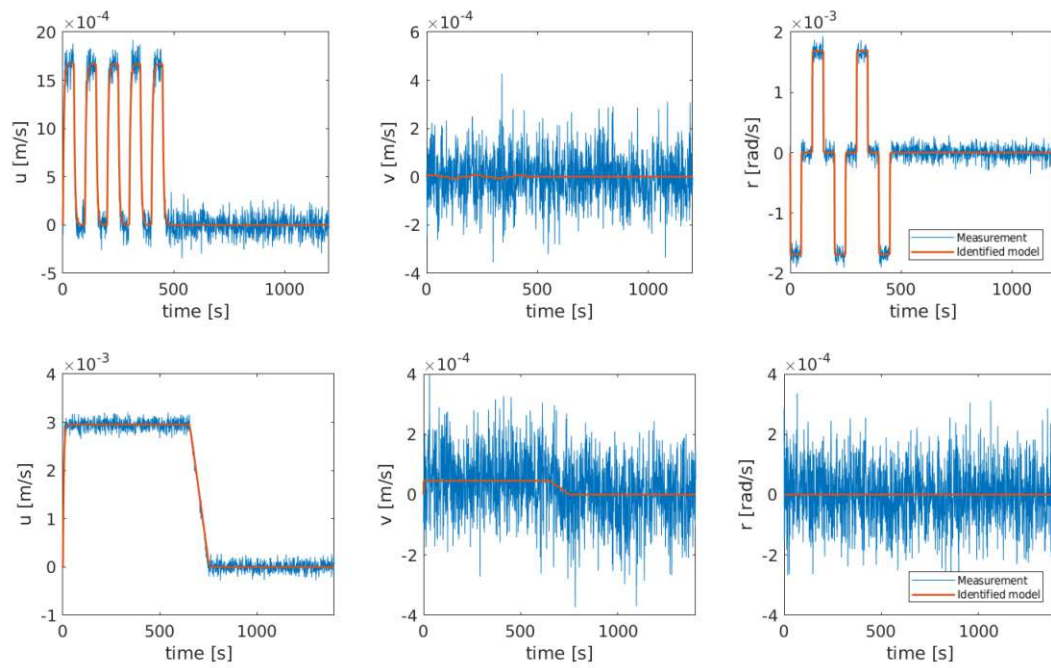


Figure 28: *A-A* identification results for two experiments.

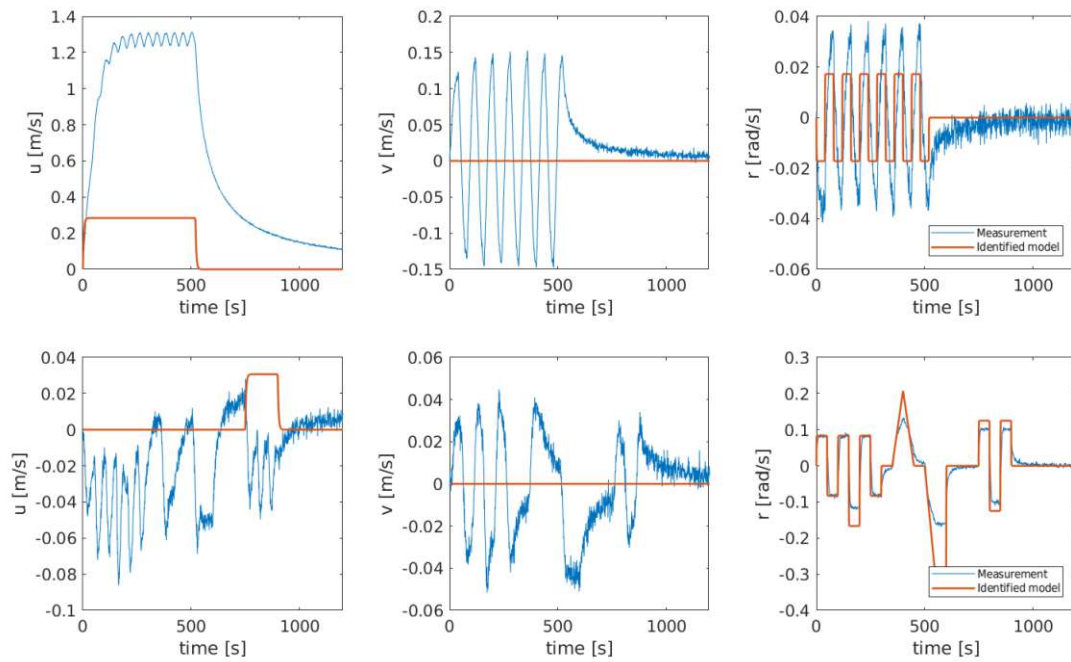


Figure 29: *A-B* inadequate identification results. In the absence of coupled hydrodynamic terms motion only happens along the axes the forces were applied to.

Model B

Again, tests were conducted to analyse whether system identification using model B provides satisfactory results when supplying data generated with model B itself. Results showing a relatively accurately parameterised model are shown in figure 30.

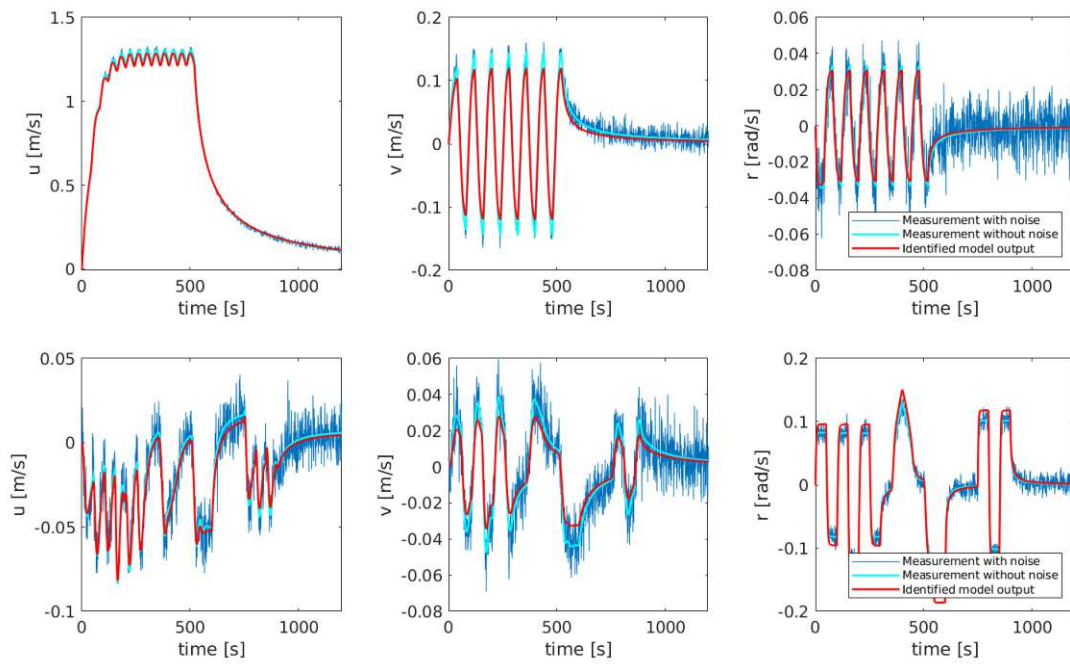


Figure 30: B - B identification results.

To test the method on independently generated measurements, a data set for the 10 experiments was generated using the "naval vessel" model from Thor Fossen's MSS toolbox. Even though the naval vessel model models its nonlinear hydrodynamic damping differently and also contains an additional degree of freedom for roll motion, model B performs adequately when used for identification. Results are shown in figure 31.

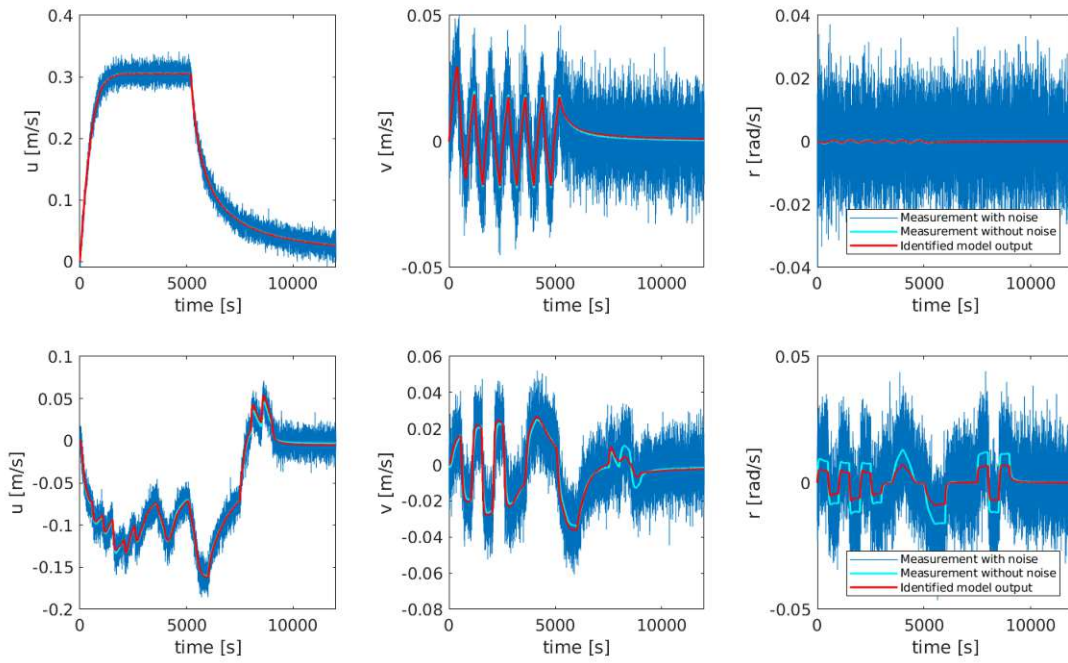


Figure 31: *B-naval vessel* identification results.

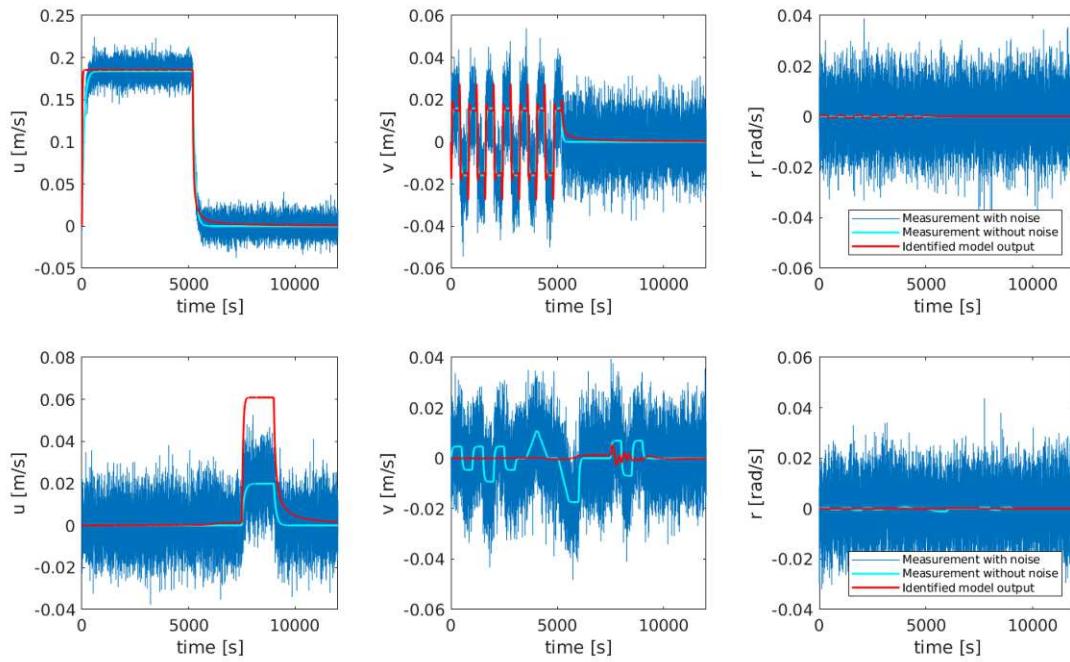


Figure 32: *B-supply ship* identification results showing insufficient ID model performance caused by inappropriate model structure.

Since model B contains only nonlinear hydrodynamic terms, problems arise when trying to perform identification on data that only contains linear dynamics. To show this limitation, results of using model B to identify the dynamics of the "supply ship" model contained in the MSS library are shown in figure 32.

Model C

To overcome the issue of only being able to identify linear or nonlinear dynamics respectively, the two formulations for hydrodynamic resistance were combined into one model C, as shown in section 2.1.3 of this thesis. This model performed well on both linear and nonlinear measurement data and is therefore used along with model B in the rest of this thesis to base the controller for the dynamic positioning system on. Results of using model C to identify the naval vessel model are shown in figure 33 and for the supply ship model in figure 34.

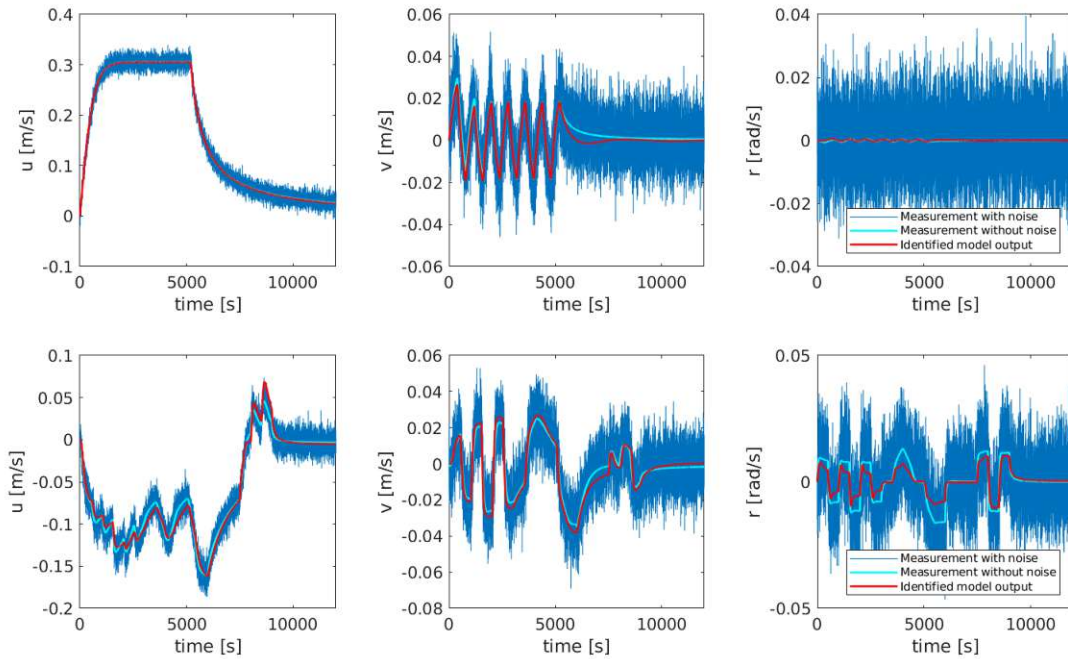


Figure 33: *C*-naval vessel identification results.

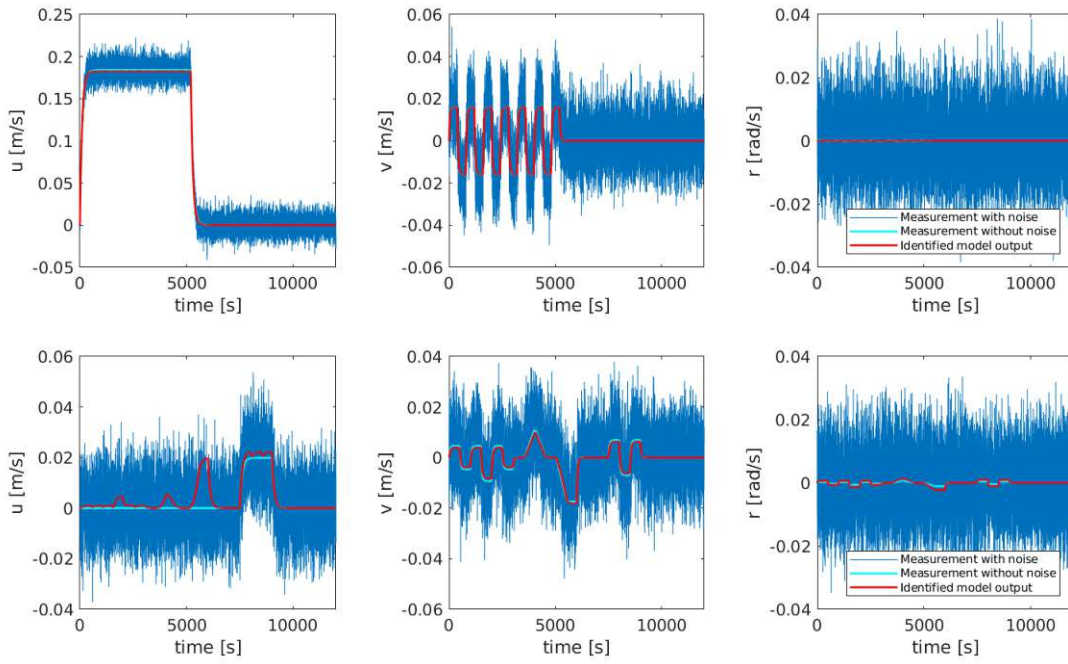


Figure 34: *C-supply ship* identification results.

2.6 System identification summary

The system identification approach of the proposed method to use identified models for controller design has been empirically validated over the previous sections. Mathematical models of linear and nonlinear structure have been implemented from literature and have been successfully parameterised for different sets of measurement data generated from models of varying complexity:

- *Model A*, containing linear hydrodynamic damping, has been shown to be suitable for identification of data generated with itself and validates the method while also showing the limitations of having insufficient model complexity.
- *Model B*, containing nonlinear hydrodynamic damping, has also been shown to successfully identify itself as well as data generated from the naval vessel model, which contains roll motions as an additional degree of freedom and nonlinear hydrodynamic assumptions.
- *Model C*, where the linear and nonlinear hydrodynamic damping terms of model A and B have been combined, has been shown to be suitable for both linear and nonlinear cases of hydrodynamic damping.

While the applied methods have theoretical limitations, they have been shown to work within a reasonable scope. For one, having data on a comprehensive set of experiments in which all parameters get sufficiently excited for the least-squares method to produce a suitable set of initial values, as discussed in section 2.4.3, is of utmost importance, otherwise the optimisation methods had been unable to produce results that adequately modeled the test models' behaviours across all degrees of freedom. Another theoretical limitation is that the required information might be lost in measurement noise. The assumptions during testing assumed SNR-values found in GPS-measurements, but solutions of this problem are of a technical nature outside the scope of this work.

Having shown the system identification approach to produce reliable results using the chosen models, the upcoming section uses models B and C as a base to illustrate the aspects and results of designing a 2-Dof controller for our test models.

3 Model based control design

3.1 General considerations

With a reasonably precise identified model, a model-based controller can be designed. The goal of this section is to outline the implemented controller and the assumed disturbances for the controller's validation. Afterwards, the results are presented and assessed.

From a control engineer's perspective, the system to be controlled can be classified as multi-input-multi-output, nonlinear and time invariant. To be able to accommodate for the nonlinearities, a 2-degrees of freedom (2-DoF) control system, consisting of an inversion based feedforward approach combined with a full-state feedback controller was implemented.

Inversion-based 2-DoF control approaches have successfully been applied to various dynamic systems and, given a sufficiently precise mathematical model of the processes in question, often reach significantly greater performance than relying solely on a feedback control system.

3.2 Control concepts

3.2.1 Pure feedforward

A classical feedforward control system, which generates a feedforward control input \mathbf{u}_* (equivalent to the ships τ_{prop}) from a desired velocity profile $\mathbf{w} = \mathbf{w}(u, v, r)$ is pictured in figure 35. Since there is no feedback loop present, the stability of the system is completely unaffected by feedforward control inputs. The lack of process feedback also means that any disturbances acting on the system cannot be taken into account, which is one of the reasons that for practical purposes feedforward systems are often combined with a feedback controller.

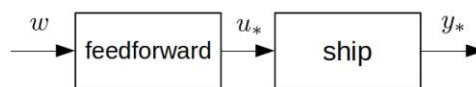


Figure 35: Feedforward control scheme.

In our implementation, the process of taking a trajectory $\mathbf{w} = \mathbf{w}(u, v, r)$ as input and calculating required forces $\boldsymbol{\tau}_{prop}$ as the control value \mathbf{u}_* for the demanded trajectory is facilitated by exact inversion of the model equations. Exact inversion is easily possible given the model structures shown in eqs. (9)-(11) and (12)-(14) and, given the results shown in the following sections, robust against parameter inaccuracies. For this approach to result in a smooth force profile, all derivatives of the control quantities required for the inversion have to be known. This is realised by using smoothstep functions for transitions between constant setpoints. For an actual implementation, the forces in $\boldsymbol{\tau}_{prop}$ can be recalculated into pod forces and angles using a constrained least-squares method as described in chapter 3.4.

3.2.2 Feedback control

For the feedback controller, a full state feedback approach with integration of the tracking error is used. The integrator plays an important role, since the fact that the identified models always contain some parameter inaccuracies leads to constant offsets for different setpoints otherwise.

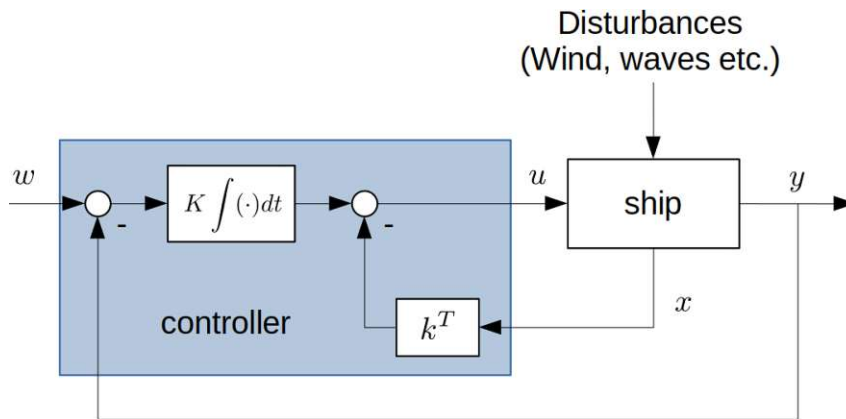


Figure 36: Full state feedback controller with integration of tracking error.

The full state feedback controller with integration of the tracking error is shown in figure 36, with the control law for finding the control input $\mathbf{u} \sim \tau_{prop}$ being:

$$\mathbf{u} = -\mathbf{k}^T \mathbf{y} + \mathbf{K} \int_0^t (\mathbf{w} - \mathbf{y}) dt \quad (16)$$

The gains \mathbf{k}^T and \mathbf{K} are found using the theory of the linear-quadratic-regulator (LQR) for a linearised system around the operating point $\mathbf{x}_0 = [0, 0, 0]$, which allows tuning of the response for each of the system outputs separately.

3.2.3 2-DoF configuration

The 2-DoF control approach combines the two concepts described above into one control system. This has the advantage of having two components with different purposes that can be tuned independent from each other: The feedforward controller is mainly responsible for the system's reference tracking behaviour, while the feedback controller concerns itself with disturbance rejection and the remaining feedforward control error.

At any moment, the feedforward system tries to establish the desired system state \mathbf{y}_* by generating the control input \mathbf{u}_* . The feedback controller then only has to consider the remaining difference between the actual state and the desired state $\mathbf{y}_* - \mathbf{y}$. This remaining deviation from the desired state can be caused by parameter inaccuracies from the identification process or caused by environmental forces acting as disturbances onto the ship.

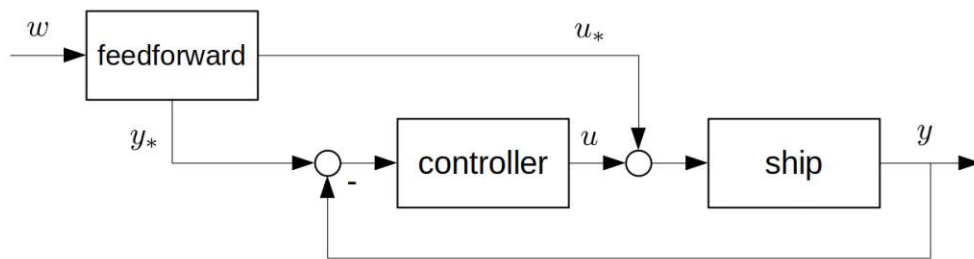


Figure 37: Feedforward control scheme.

$$\mathbf{u} = \mathbf{u}_* - \mathbf{k}^T (\mathbf{y}_* - \mathbf{y}) + \mathbf{K} \int_0^t (\mathbf{y}_* - \mathbf{y}) dt \quad (17)$$

The control law (17) uses the same gains \mathbf{k}^T and \mathbf{K} as described in the previous section.

3.3 Modeling environmental forces

To test the designed controller's performance during environmental conditions, environmental forces acting on the ship can be implemented in the simulation. These add to the forces discussed in the previous chapters and consist of wind and wave forces and ocean currents. As mentioned in chapter 2.1.1, the wind and wave forces can be added to the generalised forces $\boldsymbol{\tau}$ acting on the ship. Ocean currents on the other hand can be superimposed onto the velocity vector affecting the hydrodynamic terms, but those are excluded from this work. A mathematical model for wind forces [2] that can be used in validating the controller's performance can be implemented as

$$\boldsymbol{\tau}_{wind} = \frac{1}{2} \rho_a V_{rw}^2 \begin{bmatrix} C_X(\gamma_{rw}) A_{Fw} \\ C_Y(\gamma_{rw}) A_{Lw} \\ C_N(\gamma_{rw}) A_{Lw} L_{oa} \end{bmatrix}, \quad (18)$$

$$V_{rw} = \sqrt{u_{rw}^2 + v_{rw}^2}, \quad (19)$$

$$\gamma_{rw} = -atan2(v_{rw}, u_{rw}), \quad (20)$$

$$\begin{aligned} C_X(\gamma_{rw}) &\approx -c_x \cos(\gamma_{rw}) \\ C_Y(\gamma_{rw}) &\approx c_y \sin(\gamma_{rw}) \\ C_N(\gamma_{rw}) &\approx c_n \sin(2\gamma_{rw}) \end{aligned} \quad (21)$$

- ρ_a Density of air.
- V_{rw} Relative wind velocity.
- γ_{rw} Relative angle of attack.
- C_X, C_Y, C_N Nondimensional wind coefficients.
- c_x, c_y, c_n Approximation wind coefficients.
- A_{Fw} Frontal projected area of freeboard.
- A_{Lw} Lateral projected area.
- L_{oa} Length overall.

but according to [2] (p. 192), because of the inertia of the craft, only the mean wind forces can be compensated by the control system. In the above equations, V_{rw} is the relative velocity between vessel and wind, γ_{rw} is the relative angle of attack, L_{oa} is the length overall and A_{Fw} and A_{Lw} are the frontal and lateral projected areas. The coefficients C_X , C_Y and C_N are the nondimensional wind coefficients, which are either acquired through measurements for a specific ship, optionally resorting to using a scale model in a wind tunnel, or they can be computed numerically using semi-empirical approaches. An approximation according to [2] can be used with the approximation (21) and the numerical ranges of $c_x \in \{0.5, 0.9\}$, $c_y \in \{0.7, 0.95\}$, $c_n \in \{0.05, 0.2\}$.

While highly complex models regarding wave forces and their interactions with ship hulls exist (i.e. response amplitude operators, [14]), these forces usually consist of a slowly varying mean force and an oscillatory component. A quickly implemented model for control-testing looks like

$$\boldsymbol{\tau}_{wave} = [X_{wave}, Y_{wave}, N_{wave}]^T \quad (22)$$

$$X_{wave} = \frac{K_w^{\{x\}} s}{s^2 + 2\lambda^{\{x\}} \omega_e^{\{x\}} s + (\omega_e^{\{x\}})^2} w_1 + d_1 \quad (23)$$

$$Y_{wave} = \frac{K_w^{\{y\}} s}{s^2 + 2\lambda^{\{y\}} \omega_e^{\{y\}} s + (\omega_e^{\{y\}})^2} w_2 + d_2 \quad (24)$$

$$N_{wave} = \frac{K_w^{\{z\}} s}{s^2 + 2\lambda^{\{z\}} \omega_e^{\{z\}} s + (\omega_e^{\{z\}})^2} w_3 + d_3 \quad (25)$$

$$d_1 = w_4, \quad d_2 = w_5, \quad d_3 = w_6. \quad (26)$$

$X_{wave}, Y_{wave}, N_{wave}$	Wave forces.
$K_w^{\{x,y,z\}}$	Constants determining wave amplitudes.
$\lambda^{\{x,y,z\}}$	Parameters determining wave spectra.
$\omega_e^{\{x,y,z\}}$	Wave encounter frequencies.
w_i	Stochastic Wiener-processes.

where the wave forces are approximated using a transfer function and the stochastic Wiener-processes w_i .

3.4 Calculation of pod angles and thrusts

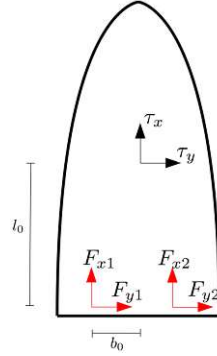


Figure 38: Force arrows and variables for calculation of pod forces.

Throughout this work, for the whole system identification and control process as well as the simulations, all forces were represented in the body-fixed reference frame and as components of the vector $\boldsymbol{\tau}$. While this streamlined the mathematical process, when determining the parameters for operation of our assumed two-pod configuration it leads to an overdetermined system of 3 equations and 4 unknowns, namely pod angles δ_p and δ_s and thrusts F_p and F_s for the port and starboard pods. To overcome this, a constrained least-squares approach ([15]) was used which solves the problem by adding the constraint, that the pods should generate a given $\boldsymbol{\tau}$ while minimising their thrust.

We formulate the problem as follows: minimise $\|Ax - b\|^2$ while demanding that $Cx = d$. The equilibrium of forces for our ship containing the pod forces

$$\text{can be written as } \begin{bmatrix} \tau_x \\ \tau_y \\ \tau_n \end{bmatrix} = \begin{bmatrix} 1 & 1 & 0 & 0 \\ 0 & 0 & 1 & 1 \\ b_0 & -b_0 & -l_0 & -l_0 \end{bmatrix} \begin{bmatrix} F_{x1} \\ F_{x2} \\ F_{y1} \\ F_{y2} \end{bmatrix} \sim \boldsymbol{d} = \boldsymbol{C}\boldsymbol{x}$$

and the condition, that the generated forces should be minimal as

$$\begin{bmatrix} 0 \\ 0 \\ 0 \\ 0 \end{bmatrix} = \begin{bmatrix} 1 & 0 & 0 & 0 \\ 0 & 1 & 0 & 0 \\ 0 & 0 & 1 & 0 \\ 0 & 0 & 0 & 1 \end{bmatrix} \begin{bmatrix} F_{x1} \\ F_{x2} \\ F_{y1} \\ F_{y2} \end{bmatrix} \sim \mathbf{b} = \mathbf{Ax}$$

A solution \hat{x} can then be found by solving

$$\begin{bmatrix} \mathbf{A}^T \mathbf{A} & \mathbf{C}^T \\ \mathbf{C} & 0 \end{bmatrix} \begin{bmatrix} \hat{\mathbf{x}} \\ \mathbf{z} \end{bmatrix} = \begin{bmatrix} \mathbf{A}^T \mathbf{b} \\ \mathbf{d} \end{bmatrix}$$

using least squares. While this approach can be extended to any propulsion configuration, it is important to consider it being a static recalculation which disregards any aspects of dynamics in the results. As with modeling the dynamics of the pods themselves, this was determined to lie outside the scope of this work. A result of this recalculation that depicts a thrusts and pod angles timeseries is shown later in section 3.7.

3.5 Feedforward performance

Performance of the feedforward controller for 3 independent trajectories are using the Dorchester Lady model, as well as the feedforward control inputs calculated through exact inversion, are shown in figure 39 and a system response for the naval vessel model in figure 40. The trajectories are a representation of speed control, lateral maneuvering for mooring and a stationary rotation. As described before, an important characteristic of feedforward systems in general is that they don't have an effect on the stability properties of the controlled process, which can be seen in the naval vessel's system response to the lateral v trajectory.

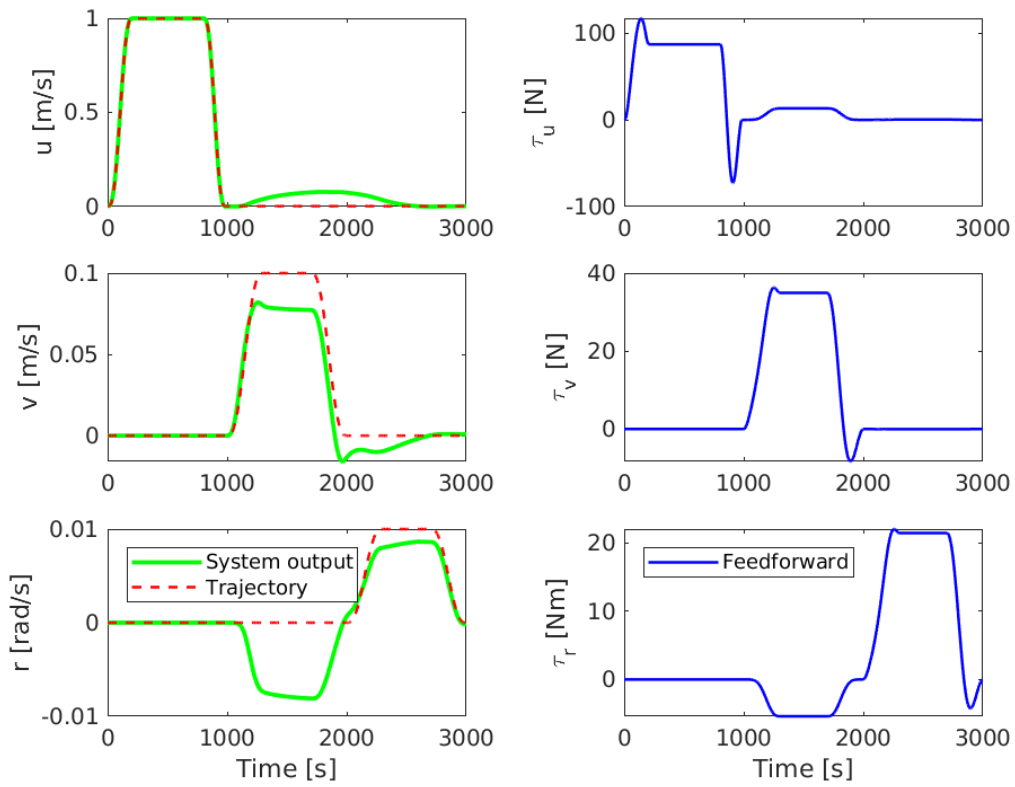


Figure 39: System output and feedforward control inputs for model B, "Dorchester Lady".

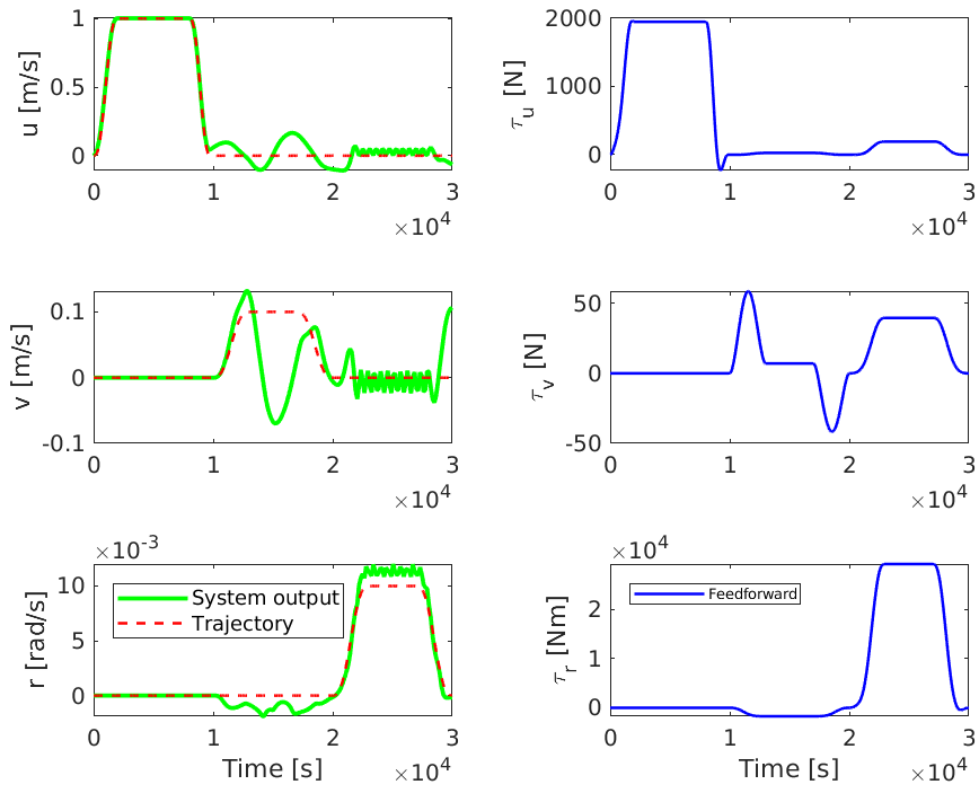


Figure 40: System output of the feedforward controlled naval vessel model. Note the effects of instability on the v -trajectory.

Figures 41 and 42 show the feedforward control system in combination with the environmental forces. These figures are shown to reiterate the point, that a feedforward control system cannot react to disturbances due to a lack of process feedback. They also show how the disturbances affect the system when trying to perform maneuvers and give a comparison between the disturbance forces to the control forces in terms of magnitude.

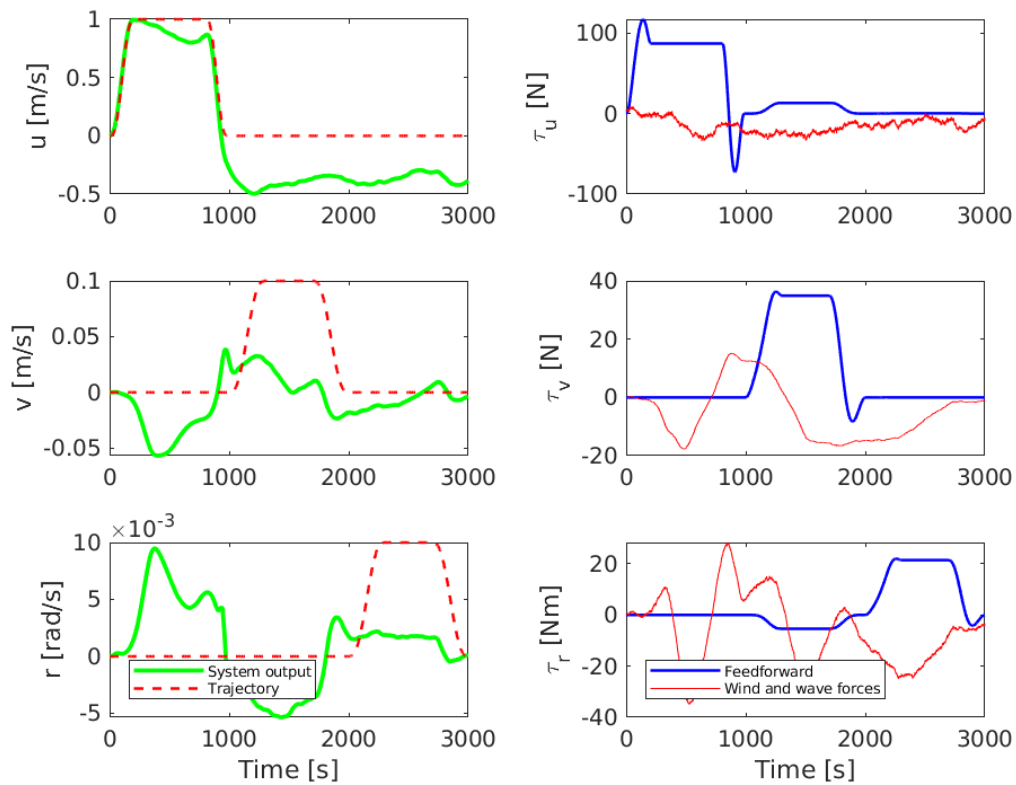


Figure 41: System output, feedforward control inputs and environmental forces for model B, "Dorchester Lady".

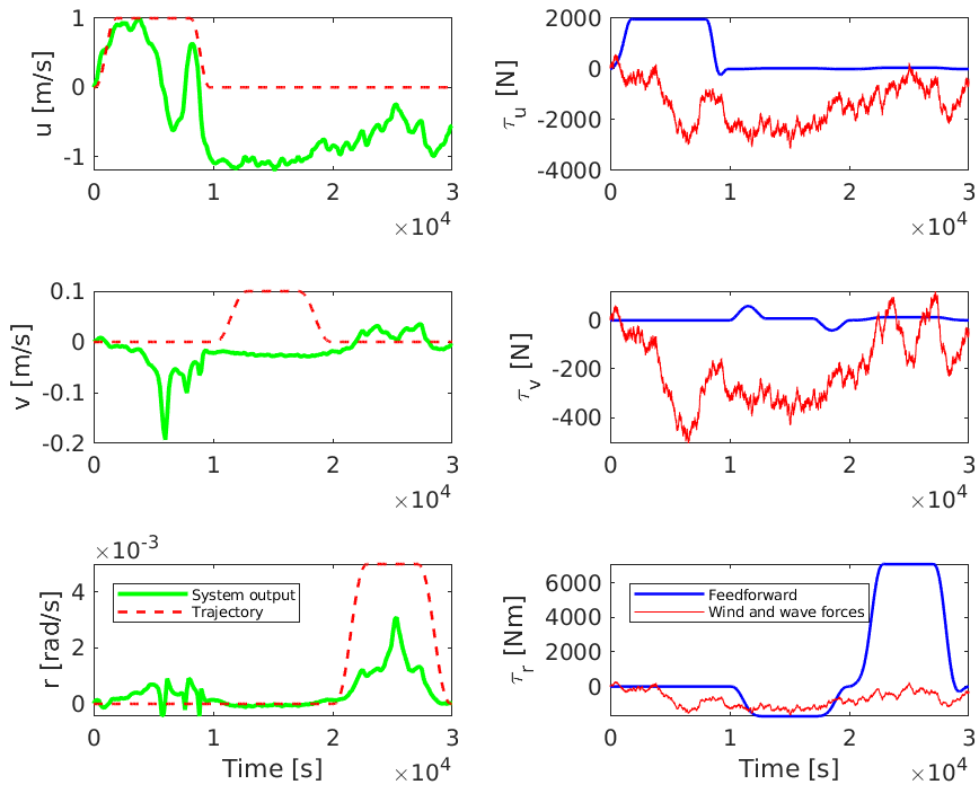


Figure 42: System output, feedforward control inputs and environmental forces for the naval vessel model.

These results show that even though parameter inaccuracies lead to slightly reduced precision and feedforward systems alone generally can't compensate for instabilities during operation, inversion based feedforward control is accurate enough to be used as a component for the 2-DoF control system.

3.6 Feedback control performance

Figures 43 and 44 show the system responses to setpoint steps along the three principal axes for the "Dorchester Lady" and naval vessel model respectively. The controllers were tuned by manually adjusting the values inside the \mathbf{Q} and \mathbf{R} matrices of the LQR approach until plausible response times were achieved.

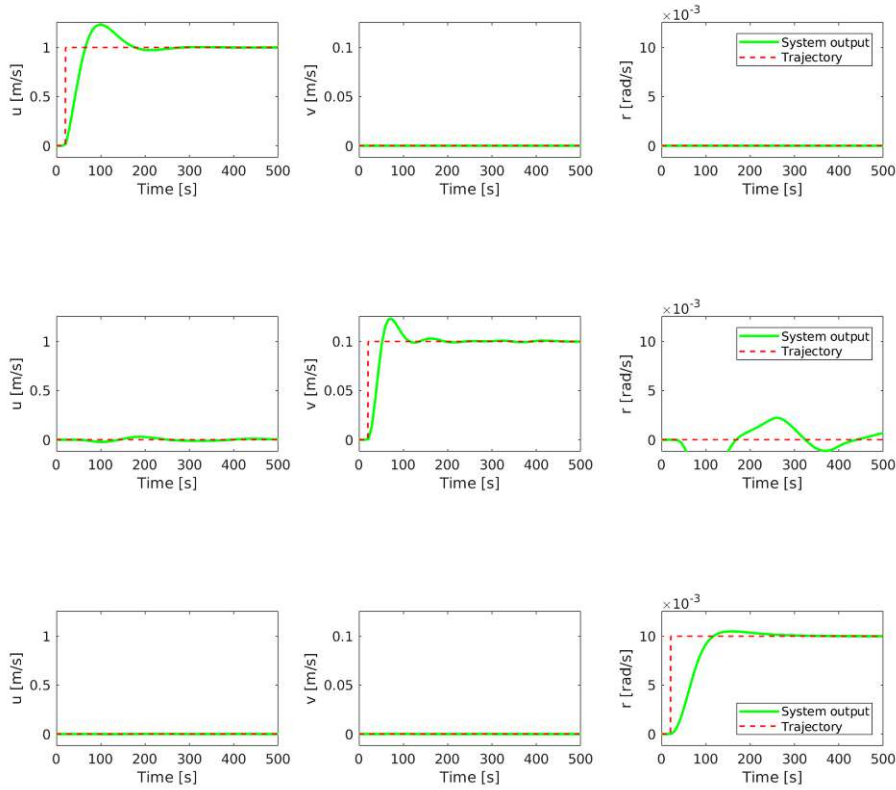


Figure 43: System responses for a setpoint-step for singular forward, lateral and rotational motion of the "Dorchester Lady" model.

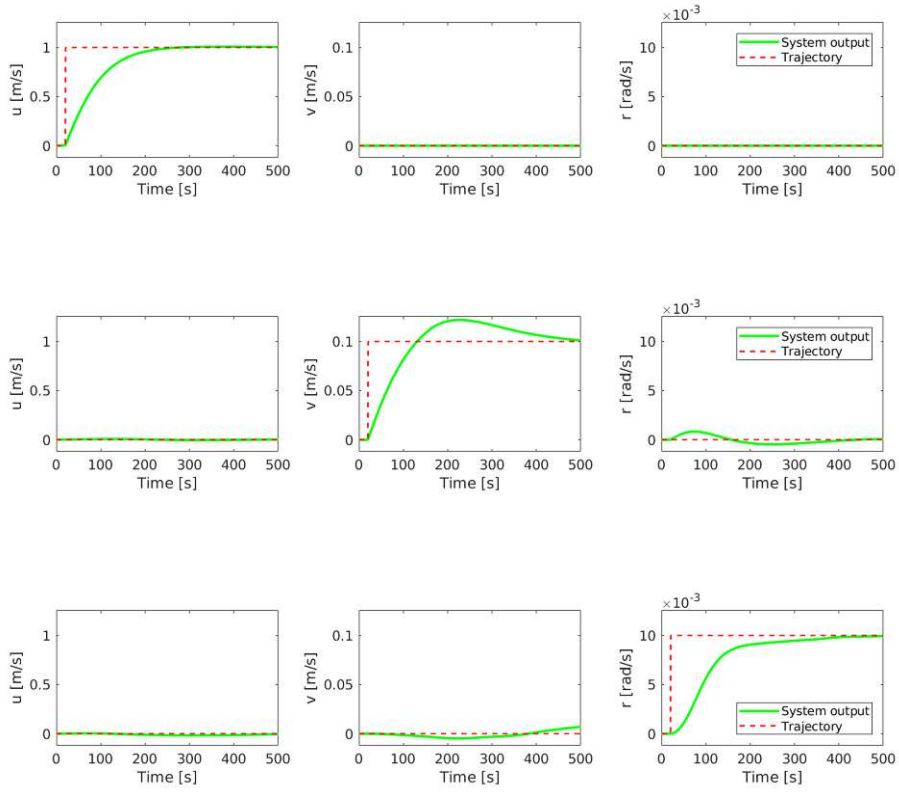


Figure 44: System responses for a setpoint-step for singular forward, lateral and rotational motion of the naval vessel model.

The simulation results show that the designed feedback controller performs adequately, again despite parameter inaccuracies. For comparability, simulation results of solely the feedback controller being tasked with performing the trajectory from section 3.5 is shown in figures 45 and 46.

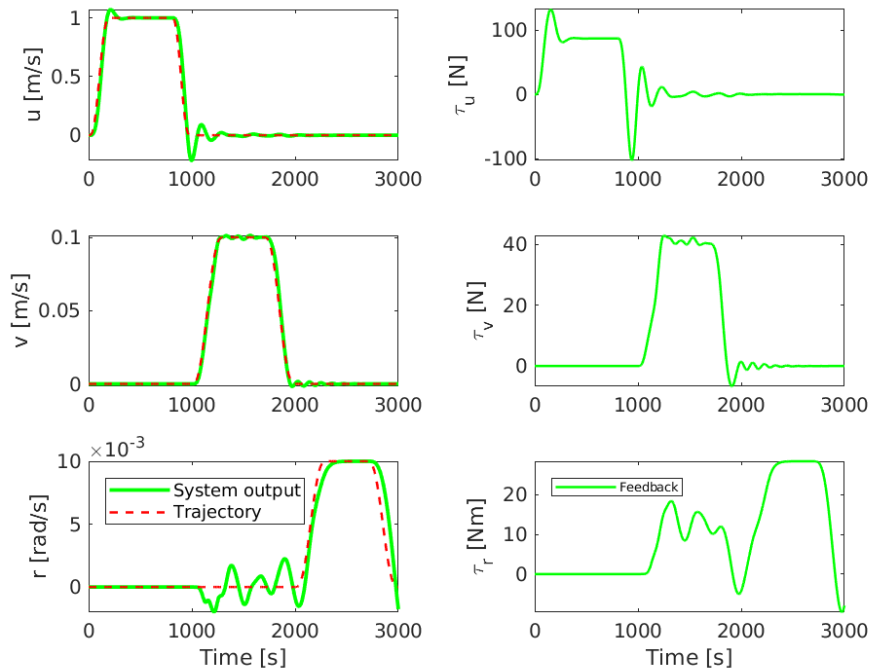


Figure 45: Performance of the full-state feedback controller of the "Dorchester Lady" model.

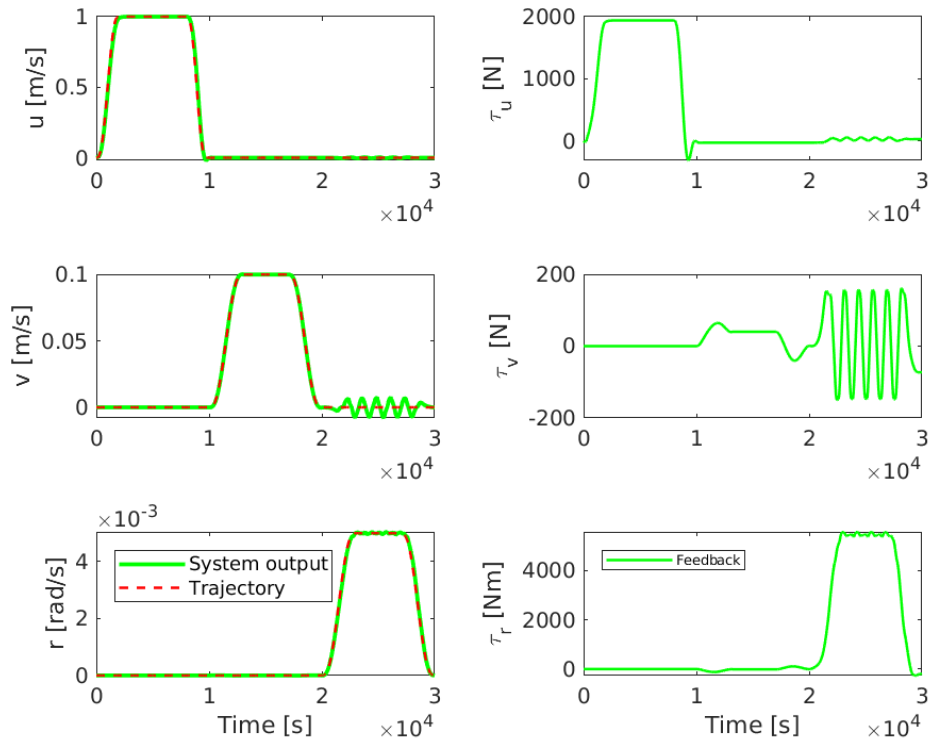


Figure 46: Performance of the full-state feedback controller of the naval vessel model.

3.7 2-DoF configuration performance

The performance of the "Dorchester Lady" model using a model B-based 2-DoF control implementation and of the naval vessel with a model C-based one are presented in figures 47 and 48. The figures show the performance gain compared to the singular components shown in the previous sections.

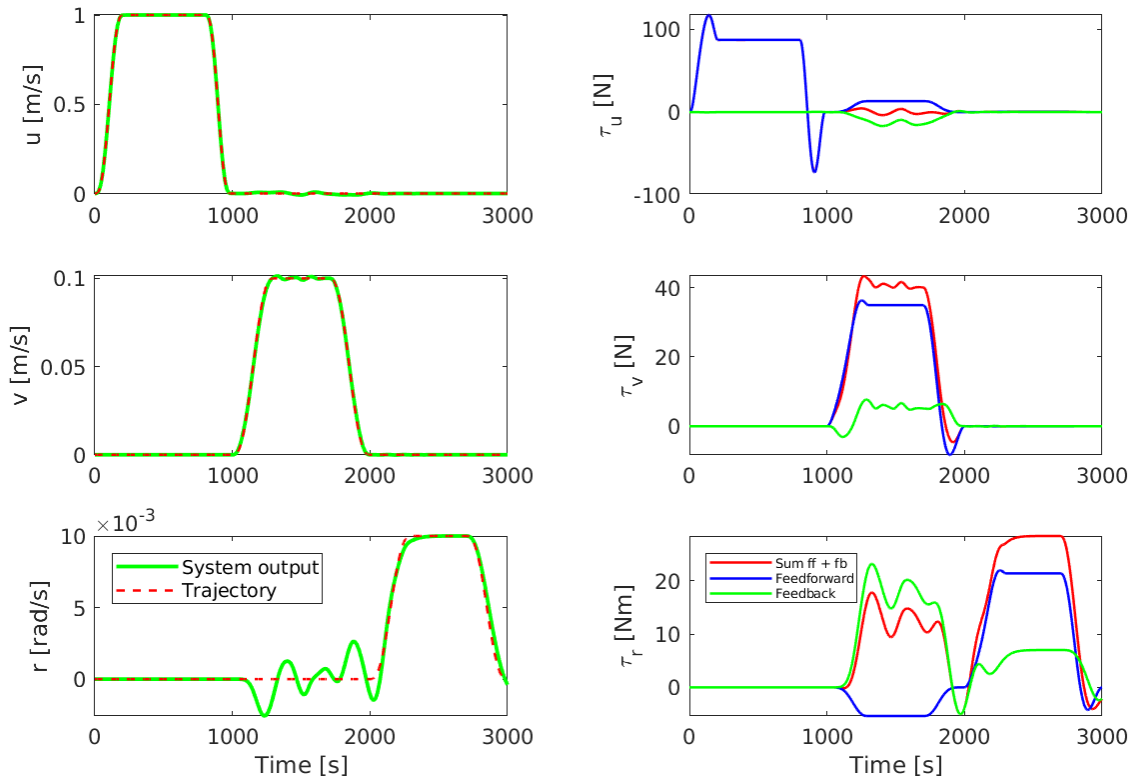


Figure 47: Performance of 2-DoF control configuration of the "Dorchester Lady" model without disturbances.

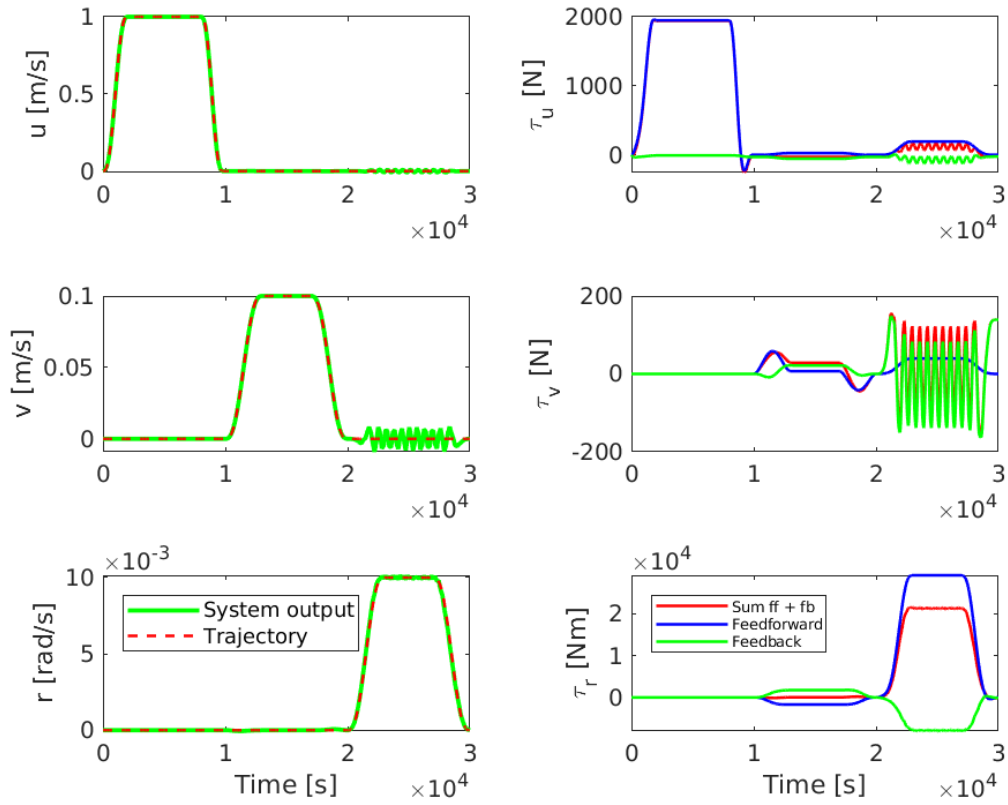


Figure 48: Performance of 2-DoF control configuration of the naval vessel model without disturbances.

Finally, the full simulations involving disturbances to test the robustness of the controller are shown in figures 49 and 50. Both tests were conducted against the wind and waves disturbance forces described in section 3.3 and using the controller gains from section 3.6. Plots of two more tests using the 2-DoF configuration and with simulated environmental forces where only the velocity profiles were supplied as trajectory are shown in figures 51 and 52. Considering the fact that the control system operates on the velocity level and errors at the position level accumulate over time, these results show a very robust performance.

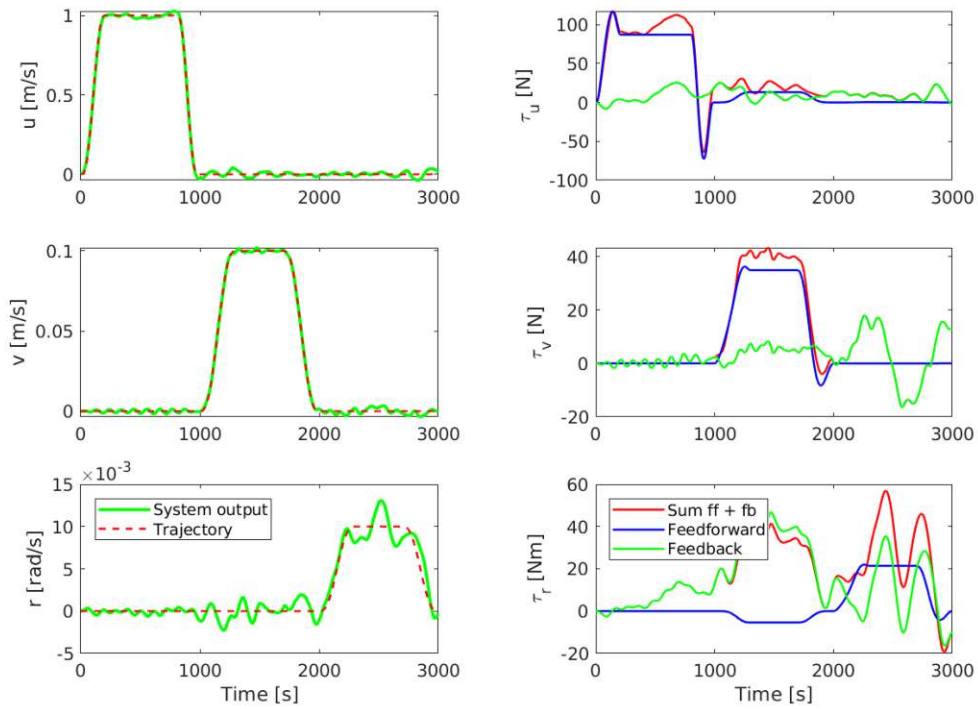


Figure 49: Performance of 2-DoF control configuration of the "Dorchester Lady" model against wind and wave forces as disturbances.

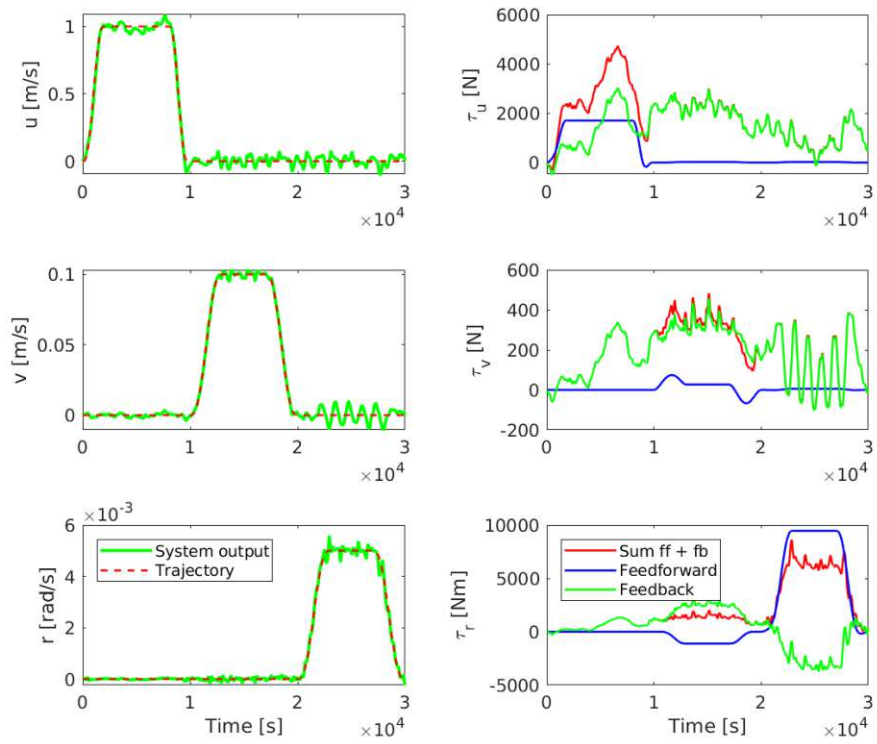


Figure 50: Performance of 2-DoF control configuration of the naval vessel model against wind and wave forces as disturbances.

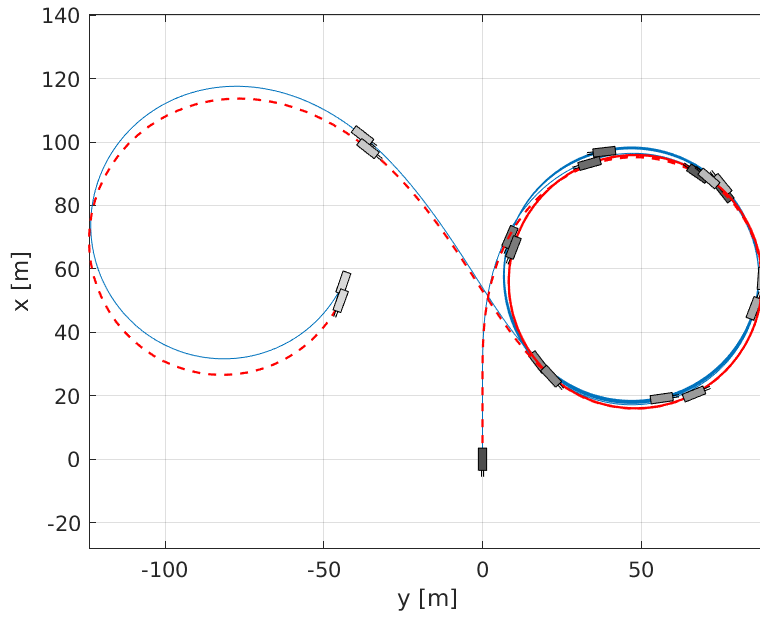


Figure 51: Integral of the supplied trajectory (red) and simulated path of the ship (blue) for the "Dorchester Lady" model in the xy -plane, 2-DoF configuration and against environmental forces.

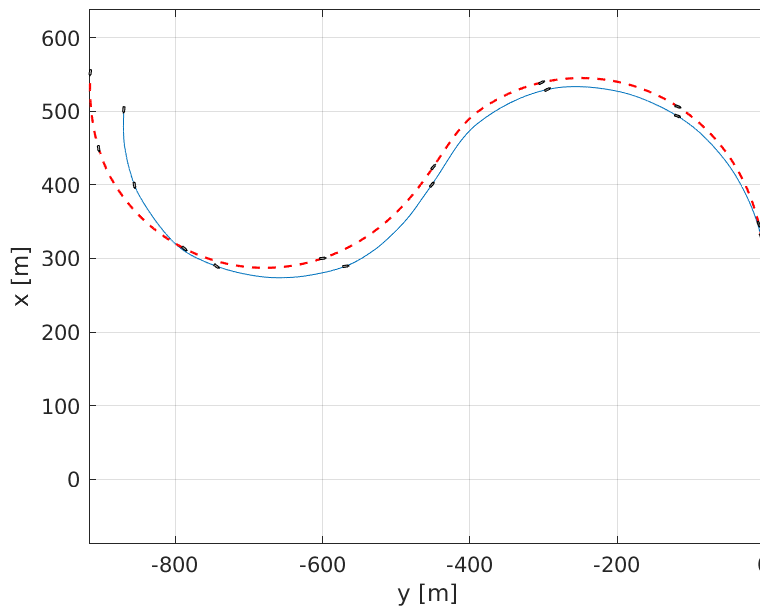


Figure 52: Integral of the supplied trajectory (red) and simulated path of the ship (blue) for the naval vessel model in the xy -plane, 2-DoF configuration and against environmental forces.

Lastly, figure 53 shows the recalculated pod forces and angles produced by the constrained least-squares method described in section 3.4 for the naval vessel trajectory shown in figure 50. While both pods perform the maneuvers and compensate for the disturbances by varying their thrusts, the pod angles δ_p and δ_s only show slight fluctuations around either 0 or π rad.

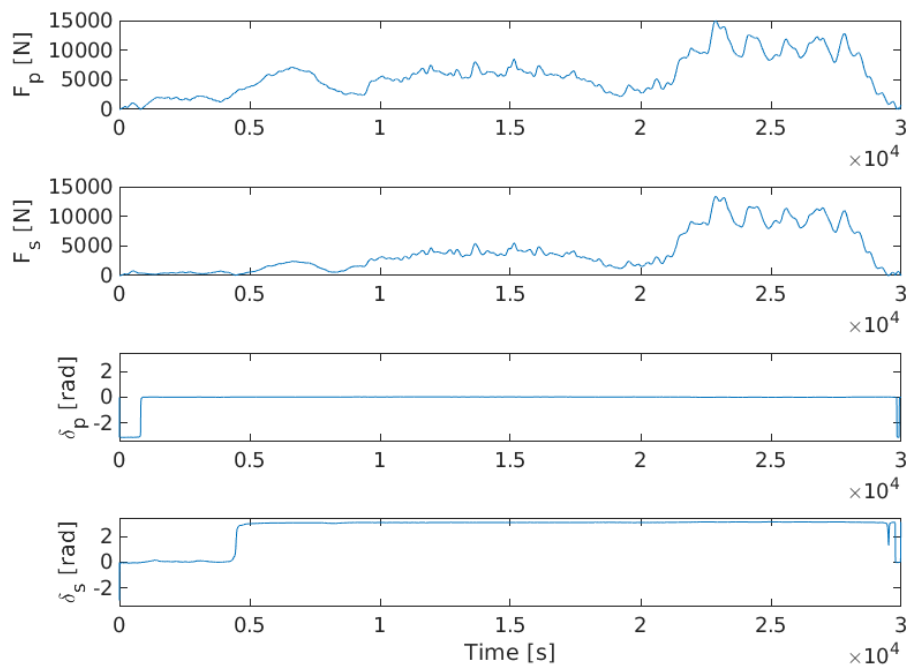


Figure 53: Exemplary pod-forces and -angles profile calculated using the constrained least squares method from section 3.4.

4 Summary and conclusion

This thesis investigated an approach for the design of a model-based dynamic positioning system for a given vessel. As a first step, the system identification process was examined in detail. Two suitable mathematical models were chosen from literature and combined into a third one. The model structure was investigated in the context of experiment design and which maneuvers have to be performed in order to be able to identify the relevant parameters. Then, the methods used for system identification, a gradient descent method combined with a least-squares based initialisation of the parameters, were analysed extensively. The results were then shown and the identified models were validated against measurement data. It has been shown that the dynamics of the test models could be approximated by applying the discussed concepts.

In addition to the findings on the system identification procedure discussed in more detail at the end of the section focusing on the topic, in the next part it has been shown in simulation that the chosen control paradigms are suitable to be applied to nonlinear ship models, even if these models are of increased mathematical complexity by containing an additional degree of freedom and higher order nonlinearities. Exact inversion was shown to be robust in the face of parameter inaccuracies. The design of the 2-DoF controller has been detailed and a way to solve the overdetermined problem of finding pod forces and angles from the generalised forces acting on the ship. Finally, the robustness of the 2-DoF controller was shown. Results from the simulations were presented in order to show the performance of each configuration of components of the 2-DoF controller and to validate the control scheme utilising models of higher complexity and incorporating environmental forces.

While the scope of the work was defined to be relatively narrow regarding the endless number of possibilities and configurations of vessels that exist in a naval context, the general approach should be applicable to most surface marine craft that adhere to the classical v-shaped hull design and provide enough degrees of freedom through their propulsion system. Since linear as well as nonlinear hydrodynamic resistances are represented, the system in theory is not limited to either low-speed or cruising speed regimes. The way propulsion was modeled was limited to a two-pod azimuth thruster configuration, but can be easily extended to accommodate for outboard motors, bow- or stern thrusters etc.

The way the propulsion forces were incorporated was also the most significant

simplification regarding the complexity of actual ship dynamics. In this thesis, the provided forces are assumed to be perfectly known, therefore further work in this area would be a logical next step for a hypothetical real-life implementation of the system. Possibilities include modeling dynamic behaviour of the pods and motors or the effects of the flows induced by the pods interacting with the pods themselves.

Regarding the control system, modifying the proposed velocity-based control into being position-based would be reasonably straightforward by adding an additional control loop on top. Further possible areas of interest could concern the way the system handles disturbances, either by investigating ways to make assumptions about these during the feedforward stage or by using model predictive control to be able to react in an optimal way to respective disturbance forces while making it easy to incorporate constraints on ship behaviour.

References

- [1] Society of Naval Architects and Marine Engineers (U.S.). Technical and Research Committee. Hydrodynamics Subcommittee. "Nomenclature for treating the motion of a submerged body through a fluid : Report of the American Towing Tank Conference", Technical and research bulletin (Society of Naval Architects and Marine Engineers (U.S.)), no. 1-5, New York : Society of Naval Architects and Marine Engineers, 1950.
- [2] T. I. Fossen, 2011, Handbook of Marine Craft Hydrodynamics and Motion Control, West Sussex, United Kingdom: John Wiley & Sons Ltd
- [3] W. Gierusz, "Simulation model of the LNG carrier with podded propulsion, Part II: Full model and experimental results", Ocean Engineering, Volume 123, 2016, Pages 28-44, ISSN 0029-8018, <https://doi.org/10.1016/j.oceaneng.2016.06.024>.
- [4] Abkowitz, M.A. (1964), Lectures on Ship Hydrodynamics – Steering and Maneuvering, Hy-5. Lyngby, Denmark: Hydro & Aerodynamic Laboratory.
- [5] W. Gierusz, "Simulation model of the LNG carrier with podded propulsion Part 1: Forces generated by pods", Ocean Engineering, Volume 108, 2015, Pages 105-114, ISSN 0029-8018, <https://doi.org/10.1016/j.oceaneng.2015.07.031>.
- [6] X. Sun, G. Wang, Y. Fan, D. Mu and B. Qiu, "Collision Avoidance of Podded Propulsion Unmanned Surface Vehicle With COLREGs Compliance and Its Modeling and Identification," in IEEE Access, vol. 6, pp. 55473-55491, 2018, doi: 10.1109/ACCESS.2018.2871725.
- [7] T. I. Fossen and T. Perez (2004). Marine Systems Simulator (MSS). URL: <https://github.com/cybergalactic/MSS>
- [8] Xue, Y.; Liu, Y.; Xue, G.; Chen, G. Identification and Prediction of Ship Maneuvering Motion Based on a Gaussian Process with Uncertainty Propagation. J. Mar. Sci. Eng. 2021, 9, 804. <https://doi.org/10.3390/jmse9080804>

- [9] Mu, D.; Wang, G.; Fan, Y.; Sun, X.; Qiu, B. Modeling and Identification for Vector Propulsion of an Unmanned Surface Vehicle: Three Degrees of Freedom Model and Response Model. *Sensors* 2018, 18, 1889. <https://doi.org/10.3390/s18061889>
- [10] Zhou, W., Liu, L., Huang, L. et al. A New GPS SNR-based Combination Approach for Land Surface Snow Depth Monitoring. *Sci Rep* 9, 3814 (2019). <https://doi.org/10.1038/s41598-019-40456-2>
- [11] Miyauchi, Yoshiki & Maki, Atsuo & Umeda, Naoya & Rachman, Dimas & Akimoto, Youhei. (2021). System Parameter Exploration of Ship Manoeuvring Model for Automatic Docking / Berthing using CMA-ES.
- [12] Weilin Luo, Xinyu Li, Measures to diminish the parameter drift in the modeling of ship manoeuvring using system identification, *Applied Ocean Research*, Volume 67, 2017, Pages 9-20, ISSN 0141-1187, <https://doi.org/10.1016/j.apor.2017.06.008>.
- [13] Taimuri, Ghalib Humayun, Jerzy Matusiak, Tommi Mikkola, Pentti Kujala and Spyros Hirdaris. "A 6-DoF maneuvering model for the rapid estimation of hydrodynamic actions in deep and shallow waters." *Ocean Engineering* 218 (2020): 108103.
- [14] Faltinsen, O. Sea loads on ships and offshore structures. United States: N. p., 1990. Web.
- [15] Stephen Boyd; Lieven Vandenberghe (7 June 2018). *Introduction to Applied Linear Algebra: Vectors, Matrices, and Least Squares*. Cambridge University Press.

Image Sources

- Fig. 1: <https://www.yamaha-motor.eu/cy/en/marine-accessories/helm-master/>
- Fig. 2: [3]
- Fig. 3: [2]
- Fig. 4: <https://www.thrustmaster.net/azimuth-thrusters/>
- Fig. 5: [3] & Mu, Dongdong, Guofeng Wang, Yunsheng Fan, Xiaojie Sun, and Bingbing Qiu. 2018. "Modeling and Identification for Vector Propulsion of an Unmanned Surface Vehicle: Three Degrees of Freedom Model and Response Model" *Sensors* 18, no. 6: 1889. <https://doi.org/10.3390/s18061889>
- Fig. 8: [7]